Controls upon the Last Glacial Maximum deglaciation of the northern Uummannaq Ice Stream System, West Greenland

Timothy P. Lane[1], David H. Roberts[1], Brice R. Rea[2], Colm Ó Cofaigh[1], Andreas Vieli[1,3], Angel Rodés[4]

[1]Department of Geography, Durham University, Science Laboratories, Durham, DH1 3LE, UK
[2]Geography and Environment, School of Geosciences, University of Aberdeen, Elphinstone Road, Aberdeen AB24 3UF, Scotland
[3] Department of Geography, University of Zurich – Irchel, Winterthurerstr. 190, CH-8057 Zurich, Switzerland
[4]NERC Cosmogenic Isotope Analysis Facility, Scottish Enterprise Technology Park, East Kilbride G75 0QF, United Kingdom

Corresponding author:

Timothy P. Lane

Email: timothy.lane@lgp.cnrs.fr

Address: Department of Geography, Durham University, Science Laboratories, Durham, DH1 3LE, UK

Phone number: +447817344057

Abstract

The Uummannaq ice stream system (UISS) was a convergent cross-shelf ice stream system that operated in West Greenland during the Last Glacial Maximum (LGM). This paper presents new evidence constraining the geometry and evolution of the northern sector of the UISS and considers the factors controlling its dynamic behaviour. Geomorphological mapping, 21 new terrestrial cosmogenic nuclide (TCN) exposure ages, and radiocarbon dating constrain LGM warm-based ice stream activity in the north of the system up to 1400 m a.s.l. Intervening plateaux areas either remained ice free, or were covered by cold-based icefields. Beyond the inner fjords, topography and bathymetry forced ice flow southwards into the Uummannaq Trough, where it coalesced with ice from the south, and formed the trunk zone of the UISS.

Deglaciation of the UISS began at 14.9 cal. kyr BP. Rapid retreat from the LGM limit was forced by an increase in air temperatures and rising sea level, enhanced by the bathymetric over-deepening of the Uummannaq and Igdlorssuit Sund troughs. Ice reached the inner fjord confines in the northern Uummannaq area by 11.6 kyr and experienced an ice marginal stabilisation in Rink-Karrat Fjord for up to 5 kyr. This was a function of topographic constriction and bathymetric shallowing, and occurred despite continued climatic forcing. In the neighbouring Ingia Fjord this did not occur. Following this period of stability, ice within Rink-Karrat Fjord retreated, reaching the present ice margin or beyond after 5 kyr. The presence of a major ice stream within a mid-fjord setting, during the mid-Holocene and the Holocene Thermal

Maximum (~11 – 5 kyr) is in direct contrast to records of other ice streams throughout West Greenland, which suggest ice had retreated beyond its present margin by 9-7 kyr. This demonstrates the potential importance of topographic control on calving margin stability, and its ability to override climatic forcing.

Keywords:

Greenland ice sheet; ice stream; deglaciation; topographic control

1. Introduction and rationale

Large ocean terminating outlet glaciers play a vital role in moderating the behaviour of Greenland Ice Sheet (GIS), as indicated by recent rapid changes in outlet glaciers dynamics (e.g. Howat et al., 2007, 2008, 2011, Holland et al., 2008, Rignot et al., 2011, Thomas et al., 2009, 2011, Joughin et al., 2012). This dynamic behaviour is typified by thinning (Rignot et al., 2011; Kjær et al., 2012) and increased discharge via calving (Howat et al., 2007) and has been closely linked to increases in air and ocean temperature, though causative processes vary and remain to be fully understood (Thomas, 2004, Howat et al., 2008, Holland et al., 2008, Nick et al., 2009, Vieli and Nick, 2011). This lack of process understanding, and short record of glacier behaviour (<20 years) makes accurate prediction of outlet glacier response to changing climate difficult.

In order to provide a longer-term record of Greenland outlet glacier behaviour, recent work has focused on the understanding of large ice streams and their influence upon the Greenland Ice Sheet (GIS) over thousand year timescales. New constraints upon ice stream extent, thickness, and deglacial behaviour from the LGM to present have been established since the early 2000's both onshore (Bennike and Bjorck, 2002, Håkansson et al., 2007, Håkansson et al., 2009, Roberts et al., 2008, Roberts et al., 2009, Roberts et al., 2010, Roberts et al., 2013) and offshore (Ó Cofaigh et al., 2004, 2013a, 2013b, Evans et al., 2009, Dowdeswell et al., 2010). These have provided evidence for the existence of large ice streams across the West, Northeast and East Greenland continental shelves during the last glacial cycle (Lykke-Andersen, 1998, Ó Cofaigh et al., 2004, 2013a, Evans et al., 2009, Dowdeswell et al., 2010).

In Greenland, it is thought that large ice streams developed through the coalescence of individual outlet glaciers in fjord settings in the coastal zone resulting in convergence and flow onto the continental shelf (Roberts et al., 2010). These large-scale, coalescent ice streams are likely to have dominated drainage from the GIS throughout Quaternary glaciations, particularly in favourable topographic or geological settings (Swift et al., 2008, Roberts et al., 2013). Based upon the presence of cross-shelf submarine troughs, it has been hypothesised that six such palaeo-ice stream systems controlled West GIS behaviour during the last glacial cycle and previous glacial periods (Roberts et al., 2010). Despite the increase in research, evidence of ice stream activity in these regions is often fragmentary, and thus far studies have been unable to provide complete on and offshore reconstructions of last glacial cycle to present ice stream behaviour. Due to their hypothesised size, ice flux, and distribution, ice streams of this scale must be understood in order to accurately reconstruct ice sheet configuration during previous glacial periods and to understand ice sheet interactions with sea level, climate, and topography.

This paper presents evidence from the northern sector of the Uummannaq Ice Stream System (UISS), central West Greenland. The aims of this paper are: (i) to present new terrestrial geomorphological and geochronological evidence from the northern sector of the UISS in order to reconstruct its LGM geometry and subsequent evolution; (ii) to use these data in conjunction with evidence from offshore and the southern sector of the UISS to understand shelf-wide ice stream dynamics during deglaciation.

2. The Uummannaq Region

2.1. Topography and geology

The Uummannaq region covers an area of ~25,000 km^2 and is highly mountainous, with summits reaching >2000 m a.s.l. (Figure 1). The region is bounded to the north and south by the peninsulas of Svartenhuk and Nuussuaq respectively (Figure 1). These landmasses form large topographic barriers, which confines the flux of ice and water from the inner Uummannaq region through the narrow passages to the north and south of Ubekendt Ejland. Within this landscape the regional-scale topography is characterised by a series of deep coalescent fjords, broadly running east to west (Figure 1). The fjord heads are occupied by marine-terminating outlet glaciers which drain the central West GIS. The fjords are of variable depth, with the majority reaching at least 500 m, and some reaching over 1100 m, and are interspersed with numerous sills and areas of localised shallow bathymetry.

Central West Greenland currently has the highest concentration of outlet glaciers in Greenland (Reeh, 1985, Velicogna and Wahr, 2006). The Uummannaq region contains 11 major outlet glaciers of varying size and discharge, the largest of which are Rink Isbræ in the north and Store Gletscher in the south. Respectively these produce 10.5-16.7 $km^3\ a^{-1}$ and 13.2-17.5 $km^3\ a^{-1}$ of ice that is calved into the ocean (Table 1) (Rignot and Kanagaratnam, 2006). Variability in subglacial topography, width, and drainage basin size is reflected in the variable ice flux they produce. Subglacial ice sheet topography in the southern Uummannaq region (areas south of Kangerlussup sermia) (Figure 1) is typically <700 m a.s.l. (Bamber et al., 2001). However, the northern Uummannaq region is bounded by an extensive sub-glacial mountain range at ~72°N (Bamber et al., 2001). The topography of this area is >900 m a.s.l., and this high terrain persists for at least 200 km inland, restricting the influx of ice from the north into the northern Uummannaq region.

The geology of the region is characterised by three distinct geological areas, separated by north to south running faults (Figure 2). The east of the region is underlain by Precambrian gneisses (Archean orthogneisses - ~2800 Ma), and forms the inner fjords (Garde and Steenfelt, 1999) (Figure 2). These are overlain by Paleoproterozoic sediments (~2000 Ma) in the north (Kalsbeek et al., 1998, Bonow et al., 2007). The centre of the Uummannaq region is formed of Cretaceous-Tertiary marine mudstones and sandstones (Pedersen and Pulvertaft, 1992, Dam et al., 2000, Henriksen et al., 2000). Finally, to the west are a series of Palaeocene basalts (61-52.5 Ma), which lie on- and offshore, forming Ubekendt Ejland, Svartenhuk, and the western half of Nuussuaq (Henriksen et al., 2000).

2.2. Current palaeo-glaciological understanding of the Uummannaq system

Until recently, the glacial history of much of the Uummannaq region was poorly known, with previous work showing the Uummannaq region to be dominated by intensely focused selective linear erosion and areally scoured terrain, with smaller isolated occurrences of valley glaciers and cold-based ice caps (Sugden, 1974). Based upon moraines, trimline elevations, and blockfields in the Svartenhuk region, a reconstructed LGM ice sheet ice thickness of 450 m a.s.l. was proposed for the northern Uummannaq region (Kelly, 1985), suggesting that ice reached just beyond Ubekendt Ejland. This estimate is considerably lower than reconstructed LGM ice thicknesses in other areas of West Greenland which are >750 m a.s.l. (Rinterknecht et al., 2009, Roberts et al., 2009). Based upon the convergent inner fjord system, and densely clustered outlet glaciers, it has recently been proposed that the region fostered a large ice stream system (the UISS) during the last glacial cycle (Ó Cofaigh et al., 2013a, 2013b, Roberts et al., 2013). The UISS extended to the continental shelf edge during the last glacial cycle, depositing sediment on the outer shelf at the trough mouth fan. This is supported by offshore bathymetry which displays evidence for a deep (>600 m) trough, containing ubiquitous, elongate bedforms indicative of fast flowing ice (Ó Cofaigh et al., 2013b).

Geomorphological data, surface exposure ages, and modelling have demonstrated that during the last glacial cycle the southern UISS ice reached a minimum of 1266 m a.s.l. in fjord head regions (Roberts et al., 2013), at least double that of earlier estimates from the northern Uummannaq region (Kelly 1985). Initial retreat from the Uummannaq trough mouth fan was underway by 14.9 cal. kyr BP (Ó Cofaigh et al., 2013b), reaching the southern inner fjords by 11.4 kyr and retreating beyond the present ice margin by 8.7 kyr (Roberts et al., 2013). This retreat is thought to have been driven by post-LGM rising relative sea-level and air temperatures, the influx of warmer oceanic water and topographic pinning throughout the inner fjords (Ó Cofaigh et al., 2013b, Roberts et al., 2013, McCarthy, 2011). Despite this new

chronology for the southern UISS, the glacial history of the northern Uummannaq region is constrained by a single radiocarbon date on eastern Svartenhuk, indicating deglaciation to the fjord margins at 10.5 cal. kyr BP (Bennike, 2000). As a result, the response of the GIS in the northern Uummannaq region to climate forcing, and its relationship to the southern sector remains unknown.

2.3. Northern Uummannaq region

The northern sector of the Uummannaq region includes fjords containing the outlet glaciers Ingia Isbræ, Umiámáko Isbræ, Rink Isbræ, and Kangerdlugssup sermerssua which discharge ice to the north of Ubekendt Ejland and into Igdlorssuit Sund (Figures 1 and 3). During the last glacial cycle, these outlet glaciers would have extended beyond their inner fjord confines, becoming confluent to the northeast of Ubekendt Ejland (Roberts et al., 2013). Bathymetric data indicates a shallow sill to the north of Ubekendt Ejland, with water depths of <100 m. This would have significantly reduced ice flow between Svartenhuk and Ubekendt Ejland (Roberts et al., 2013), forcing ice southwards into the deeper Igdlorssuit Sund. Here it would have become coalescent with ice the from southern region of Uummannaq, and flowed offshore into the Uummannaq Trough (Roberts et al., 2013).

This study focuses upon two fjords in the northern Uummannaq region, Rink-Karrat Fjord (including Rink Fjord, Karrat Fjord, and Umiámáko Fjord), and Ingia Fjord (see Figures 1 and 3). The fast-flowing outlet Rink Isbrae drains into the head of Rink-Karrat Fjord and is the highest discharging outlet glacier in the northern Uummannaq region (Rignot and Kanagaratnam, 2006). Rink Fjord is joined by Umiámáko Fjord and becomes Karrat Fjord. Rink-Karrat Fjord is a 6-10 km wide, overdeepened glacial trough, with depths reaching 1200 m close to the present ice margin. Water depths decrease to <680 m south of Karrat Island, and reach a shallow sill at <200 m north of Karrat Island. The fjord is bounded to the north and south by mountainous terrain and plateaux up to 2000 m a.s.l., with near-vertical fjord walls. High level surfaces foster small icecaps, icefields, and individual cirque and valley glaciers. Ingia Fjord is a narrow (3-6 km wide) fjord into which Ingia Isbræ calves, with a discharge of 1.1 km^3 yr^{-1}, an order of magnitude less that Rink Isbræ (10.5-16.7 km3 yr-1; Rignot and Kanagaratnam, 2006). Fjord walls are near vertical, and landsurfaces between fjords contain high level dissected plateaux ice fields up to 2000 m a.s.l. Fjord depths through Ingia Fjord are currently unknown.

3. Methods

3.1. Geomorphological mapping

Initial geomorphological mapping was carried out using 1:50,000 topographic maps, geological maps (Henderson and Pulvertaft, 1987a, 1987b), 1:150,000 aerial photographs (Kort and Matrikelstyrelsen) and ASTER GDEMs. Ground-truthing was carried out in the Northern Uummannaq region (Figure 1), where features of glacial erosion (e.g. striae, glacially smoothed bedrock, roches moutonnées and whalebacks) were mapped in order to allow palaeo-ice flow reconstructions (Glasser and Warren, 1990, Roberts and Long, 2005). Moraines and trimlines were mapped in order to constrain glacier geometry and to identify the upper ice surface/englacial thermal boundaries (Fabel et al., 2012), allowing regional ice thicknesses to be calculated (e.g. Kelly, 1985, Roberts et al., 2009). Glacial, periglacial, and fluvial landforms were mapped using a Garmin GPS 60, to accurately represent their form, length and profile (horizontal error of ±5 m, elevation error of ±5-10 m). Bathymetric estimates are derived from the local Hareø-Prøven bathymetric charts.

3.2. Terrestrial cosmogenic nuclide (TCN) dating

3.2.1. Rock sampling for terrestrial cosmogenic nuclide dating

Samples were taken for TCN dating from bedrock and erratic boulders at a variety of altitudes in order to constrain last glacial cycle ice stream geometry. Bedrock samples were taken from areas displaying clear evidence of glacial erosion (e.g. roches moutonnées or whalebacks), or from surfaces displaying striae or glacial polish to minimise the likelihood of cosmogenic inheritance (Gosse and Phillips, 2001). Samples from erratic boulders were taken when the boulder demonstrated clear evidence of subglacial erosion (i.e. subrounded to subangular; faceted, striated). Where possible, vertical sample transects were taken at altitudinal intervals of 100 m in order to provide an upper limit on warm-based ice. This was achieved on Karrat Island, with samples across the island (KA2, 6, 9, 10, 11, 15, 17, 18, 19), and in inner Rink Fjord (KA3, 20, 21, 23) (See Figure 6 for locations). However, though samples were taken this transect was limited by the number of analyses available to the project. In order to create a deglacial chronology, samples were also taken in a flow parallel transect from Karrat Island to the present margin of Rink Isbræ. To date features indicative of major ice marginal events (e.g. moraines), samples were taken from clearly glacially abraded terrain either side of the feature. Ideally samples would also be taken from boulders on the crestlines of moraines; however, due to potential problems with exhumation no boulder samples were taken from moraines. Samples were collected using a Stihl TS400 disc cutter and sampling procedures followed Gosse and Phillips (2001) and Roberts *et al*. (2013, 2008).

3.2.2. Terrestrial cosmogenic nuclide sample preparation

The sample preparation and $^{10}Be/^{26}Al$ measurement procedures used in this study are described in detail in by both Wilson *et al*. (2008) and Ballantyne *et al*. (2009). A 250 µg Be was added as a carrier to each sample in this study. A very low 10Be/Be solution from phenakite was used as carrier. This solution was provided by F. von Blanckenburg (University of Hanover) and it is widely used (see Merchel et al., 2008,). Inherent Al concentrations in quartz were determined with an ICP-MS at the NERC Cosmogenic Isotope Analysis Facility (CIAF), with a relative standard uncertainty of 3%. Al carrier was added to samples so that 2 mg Al per sample was reached. Samples KA12, KA16 and KA24 did not yield enough quartz to be processed for both ^{10}Be and ^{26}Al measurement. As a result, these are not included in this study.

3.2.3. ^{10}Be and ^{26}Al measurements and exposure age calculation

The measurement procedures at the NERC AMS laboratory are described in detail in Maden et al. (2007) and Roberts et al. (2008). $^{10}Be/^{9}Be$ and $^{26}Al/^{27}Al$ ratios were measured with the 5MV NEC Pelletron accelerator mass spectrometer at the SUERC, as part of a routine Be and Al runs. ^{10}Be and ^{26}Al concentrations are based on $2.79 \cdot 10^{-11}$ $^{10}Be/Be$ and $4.11 \cdot 10^{-11}$ $^{26}Al/Al$ ratios for NIST SRM4325 and Purdue Z92-0222 standard respectively (see Dunai and Stuart, 2009). Exposure ages were calculated using the CRONUS-Earth online calculator (Balco et al., 2009, 2008) (Calibration data set name: North-eastern North America. Calibration wrapper version: 2.2-cal-dev. Objective function version: 2.2-dev. Age calculation version: 2.1. Muon calculation version: 1.1. Constants version: 2.2), to get ages based on a sea-level high-latitude production rate of 3.968±0.15 atoms g^{-1} yr^{-1} for the 'St' scaling scheme, according to for Young et al. (2013). It should be noted that this new Baffin Bay and Arctic ^{10}Be production rate is indistinguishable from the north-eastern North America (NENA) ^{10}Be production rate (Young et al., 2013b). See Roberts *et al*. (2013) for a full description of this procedure

. Attenuation correction for sample thickness uses an attenuation length of 160 g cm-2. Topographic shielding correction is determined using the ratio of the production rate at the obstructed site to the production rate at a site at the same location and elevation, but with a flat surface and a clear horizon (Gosse and Phillips, 2001, Balco et al., 2008). The exposure ages are not corrected for past geomagnetic field variations. Including a simple palaeomagnetic correction (Nishiizumi et al., 1989) results in ages ~ 1% older ages than presented for the samples with an exposure age of ~ 10 kyr. Age determinations include a correction for atmospheric pressure related to the altitude, latitude and longitude according to the mean global surface atmospheric pressure field of the NCEP-NCAR re-analysis (www.cdc.noaa.gov/ncep_reanalysis/), but assume the standard atmosphere for geographical scaling of the production rate.

Paired ^{10}Be and ^{26}Al analysis was carried out on several samples (KA1-6) in order to test for complex exposure and shielding histories from high elevations (Gosse and Phillips, 2001). ^{26}Al/^{10}Be concentration ratios are not depleted with respect to surface production rate ratios within a one-sigma, and there is approximate concordance in ^{26}Al and ^{10}Be ages. All TCN ages are given in thousands of years (kyr), meaning thousands of years before sample collection; AD 2010 (Balco et al., 2008). TCN data is presented following the guidelines outlined by Dunai and Stuart (2009), in order to allow the use of this data in the future.

3.2. Lake coring

A number of lakes >2.5 m deep were identified from aerial photographs and chosen as targets for sediment coring. An initial series of cores were taken in order to establish the lake stratigraphy. Core samples to be used for laboratory analysis were taken using Russian-type (50 cm in length) and Eijkelkamp Beeker-type (100c m in length). A Geotek Multi Sensor Core Logger (MSCL) was then used to record core properties. Linescan images were recorded using the MSCL's line scan camera. Magnetic susceptibility was measured using a Bartington point sensor (MS2E), and gamma density was measured using a Caesium-137 gamma source.

3.3. Radiocarbon dating

Material for radiocarbon dating was sub-sampled from lake cores in Karrat Lake and Ingia Lake. Radiocarbon analysis was carried out by the NERC Radiocarbon facility (samples KaL1 and InL1). Results presented have been corrected to δ^{13}C VPDB‰ -25 using δ^{13}C values measured for each sample. The δ^{13}C values were measured on a dual inlet stable isotope mass spectrometer (Thermo Fisher Delta V) and represent the δ^{13}C in the original, pre-treated sample material. InL1 was composed of plant macrofossils and KA1 and SV1 of lake gyttja. Both were sampled from above the contact with lower minerogenic clays and overlying organic lake gyttja in their respective cores. Radiocarbon ages are presented as a 2σ range of calibrated years before present (cal. yrs BP). Ages were calibrated using OxCal 4.2 and the IntCal09 calibration curve. The lakes samples do not lie within a carbonate catchment, and as a result no reservoir correction was applied.

3.4. Bayesian analysis of deglacial chronology

In order to rigorously constrain the deglaciation of the northern UISS, Bayesian statistics were applied. This approach allows chronological information to be combined in a probabilistic nature, using prior knowledge (Bronk Ramsey, 2008). This incorporates chronological data

with information about the distance from present ice margin (or more conventionally, depth down a sedimentary profile). Through Markov Chain Monte Carlo (MCMC) sampling this forms a probability distribution of dates through the sequence (Gilks et al., 1995, Bronk Ramsey, 2009). These are expressed as age cumulative probability functions representing the likelihood of each sample's age (Bronk Ramsey, 2009). Bayesian analysis of chronological sequences has widely been used to provide coherent frameworks for radiocarbon dates through sedimentary sequences (Gilks et al., 1995, Bronk Ramsey, 2009), however, it is not commonly used for constraining a deglacial chronology (Chiverrell et al., 2013). Despite this, the principles of constraining a deglacial transect are similar to a sedimentary sequence, with distance from present ice margin substituted for depth through a profile. Their age probability distribution can therefore be used with their "stratigraphic" position (i.e. distance from ice margin) to constrain the age model. For this study, a Poisson Sequence has been used, as it allows for flexibility, permitting the depositional/retreat process to be inherently random (Bronk Ramsey, 2008), though with a given position for each age.

4. Results

Results are presented by fjord location: Rink-Karrat Fjord; and Ingia Fjord. Due to the complexity of the data from Rink-Karrat Fjord, this has been subdivided into four geographically distinct regions within the fjord: inner Fjord; Qeqertarssuaq; Nuugaatsiaq; and Karrat Island (see Figure 3). These sections outline both geomorphological and chronological results from the study.

4.1. Rink-Karrat Fjord: inner fjord

4.1.1. Geomorphology

In the inner fjord areas below 700-800 m a.s.l. were dominated by intense areally scoured terrain, displaying ubiquitous features of glacial erosion (roches moutonnées, p-forms, striae and glacially abraded surfaces) (Figures 3, 4a, 4b). A poorly developed moraine was identified at ~740 m a.s.l., formed of sub-angular gravel which contained abundant erratic quartzite material (Figure 4c). Two sets of small (6-10 m in width, 2-4 m high, and >500 m in length), poorly developed lateral moraines were mapped on the spur between Rink and Umiámáko Fjords (Figure 5). One moraine set records ice activity within Rink Fjord (R1 – R3, Figures 4d and 5), and moraines run sub-parallel to one another, at 366-235 m a.s.l. The second set (Um1 – Um3) lies on the spur between the two fjords, running obliquely downhill at 192-137 m a.s.l. (Figure 5). All moraines are formed of coarse, sub-angular to sub-rounded diamictic material, containing both local and erratic lithologies. No continuations of these moraines were observed

in Umiámáko Fjord, probably due to the near vertical relief of the fjord walls. Striae mapped from bedrock surfaces below 400 m a.s.l. are sub-parallel to macro-scale fjord topography, recording ice flow northeast to southwest (Figure 4a). Striae directions from between Rink and Umiámáko Fjord show evidence for cross cutting flow across the spur, likely reflecting differential response of each margin during deglaciation.

Above 800 m a.s.l. areally scoured terrain transitioned into heavily weathered and frost shattered bedrock. Surfaces between 1000 and 1400 m a.s.l. were dominated by frost shattering, but a number of small (<10 m^2) flat, bedrock outcrops were found, displaying evidence for glacial abrasion (Figure 4e). Above 1400 m a.s.l., intact *in-situ* bedrock blocks become very rare, and the land surface characterised by autochonous blockfield (Figure 4f).

4.1.2. Chronology

Two samples for TCN dating were taken at high elevations within the inner fjord, KA3 and KA5 (Figure 6, Table 2). KA3 was a glacially smoothed bedrock surface at 1400 m a.s.l., and returned ages of 18.9±1.9 ^{10}Be kyr (Table 3), and 22.5±1.4 ^{26}Al kyr (Table 4). KA5 was taken from an *in-situ* bedrock block found within an area of extensive autochonous blockfield at 1964 m a.s.l. This returned an age of 92.0±8.8 ^{10}Be kyr (Table 3) and 96.1±2.9 ^{26}Al kyr (Table 4), suggesting the surface had experienced minimal erosion during MIS4-2. Four low elevation TCN samples were taken from the inner fjord, from 110 – 400 m a.s.l. These were three glacially abraded bedrock surfaces (KA21, KA23 and KA27) and an erratic boulder (KA20) (Figure 6). These returned ages of 6.6±1.1 ^{10}Be kyr (KA27), 5.3±0.5 ^{10}Be kyr (KA21), 5.2±0.7 ^{10}Be kyr (KA20), and 5.0±0.6 ^{10}Be kyr (KA23) (Table 3). The geomorphological and chronological data constrain the upper limit of warm-based ice during the last glacial cycle to between 1400 and 1964 m a.s.l.

4.2. Qeqertarssuaq

4.2.1. East Qeqertarssuaq: geomorphology

Qeqertarssuaq is a 165 km^2 island near the edge of the inner fjord (Figure 3). High altitude areas were characterised by an extensive frost shattered surface, with small valley glaciers found on the northwest of the island. A number of small, infrequent bedrock outcrops were found protruding from this mantling of frost shattered material (Figures 7a - 7c). In places the upper faces of the bedrock outcrops are glacially abraded, displaying striae. The largest of these bedrock outcrops was found at 1040 m a.s.l. (71.63°N 52.90°W), with striae recording ice flow directions of 173 °-353° (set 1) and 87°-267° (set 2) (Figure 8a). Detailed inspection of the striae and their cross cutting relationship was not able to resolve their chronological relationship. However, based upon an increasing degree of topographic control during deglaciation, it is

thought that striae set 1 were formed prior to set 2. Regardless of the striae age relationship, this demonstrates warm-based ice above this altitude (1040 m a.s.l.) during the last glaciation. A sample was taken from this location for TCN dating (KA24). However, once processed, there was insufficient quartz in the 125 – 500 μm size fraction to allow etching and successful beryllium recovery. A subdued, poorly developed ridge runs northeast to southwest on the southern edge of the island (Figure 8a), terminating at the edge of the broad col which covers the centre of the island. The ridge is composed of loose, angular pebbles and cobbles, dominated by local lithologies with occasional erratics. This is interpreted as a lateral push moraine, where fjord ice has overtopped the topography.

Above ~800 m a.s.l. the western flank of Qeqertarssuaq was characterised by extensive frost shattered material formed of locally derived angular to sub-angular material. Below this, lower elevation terrain fostered a series of 12 subparallel ridges, with smaller fragmentary ridges between them (Figures 7e and f – and see inset location in Figure 3). These are formed of sub-angular to sub-rounded clasts, and are clearly of different lithological composition to higher altitude scree. The highest of the ridges (ridge Q1) is found at 786 m a.s.l. and is also the most distinct, reaching 6-8 m high (Figure 7d). Upslope of Q1 is a large (5 m wide), bedrock incised channel (Figure 7d). As a result of these observations, the 12 ridges and fragments between them (found from 786 to 340 m a.s.l.) are interpreted as a lateral moraine staircase. Due to a lack of boulders displaying clear evidence of subglacial rounding, and the absence of abraded bedrock, no surface exposure samples were taken from this site.

4.2.2. Nuugaatsiaq, southwest Qeqertarssuaq

Nuugaatsiaq is an 18 km^2 low elevation (<180 m a.s.l.) and low relief peninsula on the southwest side of Qeqertarssuaq (Figure 1). The peninsula is bordered to the north by a near vertical wall rising to 1400 m a.s.l. Three ridges of varying preservation were mapped on the eastern side of the peninsula, at 10-30 m a.s.l. (N1), 55-70 m a.s.l. (N2) and 120-133 m a.s.l. (N3) (Figure 8). These were formed of diamictic material, dominated by sub-angular to sub-rounded clasts, and interpreted as a series of lateral moraines. A further, more fragmentary moraine was found at the break of slope between the peninsula and fjord wall (N4 – 260 m a.s.l.), displaying evidence of extensive post-depositional rock glacierisation (Figure 8). Moraines N1-N3 are found sub-parallel to the present coastline (Figure 8a), and continued to the northeast, following the base of the Qeqertarssuaq Island for 5km (Figure 8b). Although slopes are mantled by a thick scree cover, this is clearly discernible from the lighter coloured morainic material (Figure 8). Striae mapped from bedrock outcrops west of N3 (71.56°N 53.13°W) displayed cross cutting flow directions of 58°-238° (1) and 20°-200° (2). The first of these

suggests ice flow concordant with fjord morphology (east-northeast to west-southwest). Contrastingly, the second set of striae suggests ice overriding the region from a north-eastern source. This is similar to other ice directional indicators found at higher altitude on eastern Qeqertarssuaq.

The terrain drops in elevation to the west of N3 (Figure 8b) to a region of low relief bedrock knolls and areas of flat topped sediment infills (at ~90 m a.s.l.). Terrain rises to the north, west and southwest of this depression, enclosing a small shallow basin (~2-4 km^2). Extensive sediments at least 2 m thick were found throughout the depression, bounded to the east by moraine N3. Some evidence of cryoturbation is present in the upper 30 cm of the sequence, but the majority of sediments are characterised by interbedded fine sand and clayey silt, displaying un-deformed, *in-situ* planar and ripple cross bedding. The sediments appear well-sorted, with few granules and no pebbles, suggestive of a relatively low-energy depositional environment. The sediments show no deformation (other than cryoturbation), suggesting deposition following the most recent regional deglaciation. Geomorphological and sedimentological evidence suggests that the sediments were deposited in a glacio-lacustrine setting as deltas, in a basin constrained by higher topography to the west of the peninsula, and by the N3 moraine to the east (Figure 8a). A series of small breaches were found incised through N3 and are likely to have been caused by a series of lake drainage events, resulting from filling to the level of the moraine crest and subsequent drainage of the lake. The breaches have then been filled by small braided stream systems.

4.3. Karrat Island

4.3.1. Geomorphology

Karrat is a 56 km^2 island, close to the outer margin of Rink-Karrat Fjord (Figures 1 and 3). It divides the fjord into two narrow channels, 3.4 km and 5 km wide respectively. The island has a low relief, low elevation eastern end (<300 m a.s.l.), which rises steeply to a 950 m a.s.l. bedrock ridge in the centre (Figures 9a and b). Ridge summits were covered by shattered bedrock, with a thin cover of autochthonous blockfield and partially shattered bedrock. In some places on the summit, large (~9 m^2) slabs of intact, *in-situ* bedrock were present (Figure 9b), though no striae were found. The near vertical ridge walls showed some subtle abrasion and smoothing, suggesting erosion by warm-based ice cover. The low elevation eastern end of Karrat was characterised by areally scoured terrain, with glacially smoothed bedrock and roches moutonnées, interspersed with small (100-300 m wide) shallow (3-5 m) lakes (Figure 9c). A series of three inset ridges were found on the north and eastern sides of Karrat (Figure 10). They were formed of coarse (cobble to boulder), angular to sub-rounded, diamictic material.

The ridges are interpreted as a series of inset lateral moraines (K1 – 49m, K2 – 137m, K3 – 210 m a.s.l.) (Figures 9d, 9e, and 10). K3 is the largest and most extensive of the moraines (4m in height, and 15m in width), (Figures 9d and 9e). These are interpreted as the southern counterpart of the Nuugaatsiaq moraines, representing the lateral portions of a latero-frontal moraine system to the north of Karrat.

Glacial bedforms are ubiquitous both inside and outside of the Karrat moraine complex. These are dominated by roches moutonnées, with some whalebacks (7% of measured bedforms). The majority of bedforms display unidirectional striae (108°-288°), however, a number show evidence for cross cutting ice flow (32°-212° (set 1), 77°-257° (set 2) and 108°-288° (set 3)), and multiple plucked faces (Figures 9f and 10). Detailed analysis of the striae was not able to robustly constrain their age relationship. However, on the interpretation of a progressive increase in topographic control on ice flow direction during deglaciation, their relative chronology is thought to be set 1 (oldest) to set 3 (youngest).

4.3.2. Chronology of Karrat Island

The highest elevation TCN sample was KA2 (724 m a.s.l. – see Figure 5, Table 2), taken from an *in situ* bedrock slab, returning ages of 11.7±1.2 ^{10}Be kyr (Table 3) and 13.5±2.2 ^{26}Al kyr (Table 4). The ^{10}Be and ^{26}Al age determinations are overlapping within error, suggesting a robust age for the sample, and the overriding by erosive ice at this altitude during the last glacial cycle.

A series of samples were taken across the east of the island. Sample KA9 (482 m a.s.l. – see Figure 6) returned a date of 12.1±1.2 ^{10}Be kyr (Table 3) and 11.6±1.0 ^{26}Al kyr (Table 4). Samples KA6, KA10, and KA11 also lie outside the moraines (Figure 6), and returned ages of 11.9±0.8 ^{10}Be kyr, 7.2±0.6 ^{10}Be kyr/8.3±0.9 ^{26}Al kyr, and 9.1±0.9 ^{10}Be kyr/11.5±1.5 ^{26}Al kyr respectively (Tables 3 and 4). These provide a maximum age for moraine formation. Samples KA15, KA18, and KA19 are situated between moraines K3 and K2 (Figure 6), and returned ^{10}Be ages of 2.2±1.3 kyr, 3.4±0.3 kyr, and 6.5±0.5 kyr respectively (Table 3). Finally, sample KA17 was taken from glacially abraded bedrock between moraines K2 and K1 (Figure 6), returning an age of 6.9±0.7 kyr (Table 3).

The aforementioned samples KA15 and KA18 were not included in analysis of the results. Their ages (2.2±1.3 kyr and 3.4±0.3 kyr respectively) appear anomalously young, and are incompatible with a large number of other dates from Karrat, and Rink Fjord (KA16, KA17, KA19, KA20, KA21, KA23, and KA27). Both excluded samples were taken from sloping bedrock surfaces, with local spreads of morainic material. The anomalously young ages of these samples

in comparison to the rest of the dataset suggest that the locations have only become exhumed recently (Putkonen and Swanson, 2003). Alternatively, if the two excluded samples are correct and represent exposure following a Neoglacial readvance at ~3.4 kyr, ice would have had to retreat to a position up-fjord of sample KA23, by ~5.2 kyr, and then readvance without causing further subglacial erosion of samples KA23 and KA27, and without destroying erratics KA17, KA19 and KA20). Furthermore, sites of KA15 and KA18 would have to have been eroded and cosmogenically reset while KA20, KA27, KA17 and KA19 remained uneroded - this is scenario is implausible Also pertinent to this argument is the regional Neoglacial readvance limit, which, within West Greenland is widely acknowledged to be the Little Ice Age limit (Kelly, 1980, Funder et al., 2011). In the case of Rink Isbrae this is only 4 km west of the present ice margin and some 35km from Karrat Island suggesting that samples KA 15 and KA 18 are anomalously young.

Further constraint upon the deglacial chronology is provided by a ^{14}C age from Karrat Lake, a small lake on the low-level surface on eastern Karrat clearly outside the K3 moraine (71.51° N 52.95° W, Figures 9a and 10). A 1 m sediment core was retrieved from the centre of the lake, containing two lithofacies; a minerogenic sandy clay (LF-K1) overlain by an organic lake gyttja (LF-K2) (Figure 11). In addition to the visual stratigraphy, the transition from LF-K1 to LF-K2 is marked by a rapid decrease in magnetic susceptibility and an increase in porosity. This suggests a rapid transition from dense, minerogenic material (LF-K1) to a highly organic, porous material (LF-K2). LF-K1 is interpreted as distal glacio-lacustrine sediment, dominated by glacially derived rock flour input, thus recording the last retreat of ice from the site. A bulk gyttja sample was taken from 1 cm above the LF-K1 to LF-K2 transition for ^{14}C dating (sample - KaL1), returning an age of 11196-11316 cal. kyr BP (2σ range) (Table 5). This date represents a minimum age for deglaciation from this point, and is in agreement with the local TCN deglacial dates from this area (KA1, KA4, and KA6).suggesting there are no issues relating to age overestimation (Wolfe et al., 2004).

4.4. Ingia Fjord

4.4.1. Geomorphology

Fjord walls along Ingia Fjord were glacially smoothed up to 800-1000 m a.s.l. Above this, the terrain was mantled by extensive scree, autochonous blockfield, and weathered bedrock surfaces. The boundary between these terrain types is marked by a faint trimline (Figure 12a). The majority of work in Ingia Fjord was carried out on a small (24 km^2) peninsula, 15 km from the present ice margin. The low elevation peninsula was characterised by low relief hilly

topography, with ubiquitous roches moutonnées, whalebacks, and small lakes (Figure 12b). Bedform long axes were broadly concordant with striae directions and fjord topography, recording northeast to southwest ice flow (64°-244° see Figure 12b). A large (10-30m high), discontinuous moraine ridge was mapped at 420-446 m a.s.l., close to the break in slope at the steep fjord wall (Figure 12a). The ridge is composed of sub-angular to sub-rounded clasts from local lithologies, with some occasional erratic material. In places it appears to have undergone some post-depositional rock glacierisation.

4.4.2. Chronology of Ingia Fjord

The surficial geology of this area is dominated by metagreywackes characterised by very thin bedding planes and high joint densities. However, these were very low in suitable quartz, and potentially dateable surfaces were often highly fragmented and unsuitable for dating. Chronological control for deglaciation through Ingia Fjord is reliant upon a single ^{14}C age from Ingia Lake (IL1), a 200 m^2 lake at 262 m a.s.l. on the Ingia Fjord peninsula (71.86° W 53.03° W) (Figure 12a). A 0.97 m sediment core was taken from the centre of the lake, displaying two lithofacies; an unconsolidated silty sand to clay (LF-I1), overlain by a partially laminated, highly organic lake gyttja with common detrital macroscopic plant remains (LF-I2) (Figure 11). This sedimentological switch is accompanied by a rapid drop in magnetic susceptibility and increase in porosity at the boundary between LF-I1 and LF-I2. As in Karrat Lake, LF-I1 is interpreted as a fining upwards glacio-lacustrine deposit, formed by sedimentation into a body of standing water, following local ice retreat. A sample of macroscopic plant remains was taken for ^{14}C dating from 1 cm above the contact between LF-I1 and LF-I2, yielding an age of 9.7-9.9 cal. yrs BP, thereby providing a minimum age for the deglaciation of Ingia Isbræ to this mid-fjord position.

5. Discussion

5.1. Configuration of the northern UISS during the last glacial cycle

Both geomorphological mapping/data and surface exposure ages provide compelling evidence for erosive warm-based ice throughout the inner fjords of Rink-Karrat, Umiámáko, and Ingia Fjords during the last glacial cycle. Ice thicknesses throughout the inner fjord region reached >1400 m a.s.l., but remained below 1968 m a.s.l., as constrained by KA5. Some overtopping of fjord topography occurred between 1000 and 1400 m a.s.l., but high level plateaux between troughs (>2000 m a.s.l.) prevented the overwhelming of regional topography by unconfined, diffluent ice during the last glacial cycle. These high level areas are presently covered by blockfields or small plateau icefields. At the LGM they would have either remained exposed as

nunataks, or become covered by cold-based ice as icefields expanded. $^{10}Be/^{26}Al$ isotope determinations from the only sample above 1500 m a.s.l. (KA5) suggest no inheritance, and therefore ice-free conditions throughout the last glaciation. However, in order to fully understand ice coverage of high-altitude plateaux, a more rigorous programme of surface exposure sampling from these altitudes would be necessary. Similar results are found from high altitude surfaces in southern Uummannaq (Roberts et al., 2013), with blockfield suggesting either ice free or cold-based ice cover during the last glacial cycle. Concordance of ^{10}Be and ^{26}Al ages throughout samples below 1000 m a.s.l. suggests sufficient erosion of bedrock to prevent inheritance (Tables 3 and 4).

Based upon geomorphological and surface exposure data, ice thicknesses in the vicinity of Karrat Island were at least 720 m a.s.l., though ice is thought to have submerged Karrat Island (900 m a.s.l.). Ice from Rink and Umiámáko Isbræ would have become confluent to the east of Karrat Island, with Rink Isbræ forcing Umiámáko Isbræ over the centre and east of Qeqertarssuaq (as evidenced by striae – see section 4.2.1). Once ice from Rink-Karrat Fjord reached the east of Qeqertat Imát, it became confluent with ice from Ingia Fjord. Ocean floor bedforms provide evidence for highly convergent flow into the Uummannaq Trough, from the east and north (through Igdlorssuit Sund) (Ó Cofaigh et al., 2013b). A shallow sill between northern Ubekendt Ejland and southern Svartenhuk (<200m below sea level) would have aided this, acting as a topographic barrier to ice moving west, and it has been hypothesised that ice was drawdown southwards through Igdlorssuit Sund (Roberts et al., 2013). Once coalescent, the southern UISS itself would have continued to drawdown ice from the northern UISS, further enhancing the southerly flow through Igdlorssuit Sund.

Although ice thicknesses during the last glacial cycle were comparable between the north and south UISS, outlet glaciers in the northern UISS remained within their fjord confines during the last glacial cycle, separated by high elevation plateaux (>2000 m a.s.l.) that would have remained as ice free nunataks or, more likely, covered by cold-based ice caps. In contrast, plateaux elevations in the southern UISS (north of Nuussuaq) are <1000 m a.s.l., and not of sufficient altitude to keep outlet glaciers within their fjord confines during the last glacial cycle. As a result of this extensive diffluent flow, Roberts *et al*. (2013) proposed a progressive westward migration of the southern UISS onset zone through the last glacial cycle. This occurred as ice thicknesses increased and topographic controls within the inner fjord region became less influential on overall ice dynamics (Roberts et al., 2013). As a result, larger-scale regional topography (e.g. Nuussuaq, Svartenhuk, and Ubekendt Ejland) would have become the principal topographic controls upon flow routing. In contrast, the outlet glaciers in the northern

UISS appear to have remained within the confines of the local fjord topography and, hence, predicting any degree of onset zone migration during the last glacial cycle is difficult.

5.2. Deglaciation of the northern UISS; timing, retreat style, and controls

In combination with geomorphological and chronological data from the offshore and southern sectors of the UISS (Ó Cofaigh et al., 2013b, Roberts et al., 2013), this work provides the first complete reconstruction of the UISS' LGM geometry and the chronology of its subsequent deglaciation (Figure 13). The palaeo-UISS contains all diagnostic components of an ice-stream in both contemporary, and palaeo settings (Stokes and Clark, 1999): individual outlet glacier tributaries; a convergent onset zone; streamlined bedforms; and a trunk zone which feeds into a large trough mouth fan at its terminus. A time-distance path for the retreat of ice through Rink-Karrat Fjord is presented in Figure 13c and this framework is used to explore the regional forcing mechanisms driving deglaciation (Figure 14).

5.2.1. LGM limit to Ubekendt Ejland

The LGM deglaciation of the UISS from the shelf-edge is discussed by Ó Cofaigh et al. (2013b), with retreat from the continental break underway by 14.9 cal. kyr BP. Surface exposure dates from Ubekendt Ejland, record ice retreat and thinning to the south east of Ubekendt Ejland by 12.4 kyr (Roberts et al., 2013). A lateral moraine sequence between 670 and 125 m a.s.l. on southern Ubekendt Ejland provides for top-down thinning and ice margin retreat occurring simultaneously (Roberts et al., 2013). This retreat from the shelf edge (14.9 cal. kyr BP) is coincidental with the onset of Greenland Interstadial 1e (14.7-14.1 GICC05 b2k - Figure 14) (Lowe et al., 2008), a period of increasing insolation (Huybers, 2006), and rising sea-level in West Greenland (Figure 14) (Long et al., 1999, Simpson et al., 2009). Reconstructions of ocean temperature on the Uummannaq shelf suggest that the warm West Greenland Current (WGC) only entered the Uummannaq Trough after 8 cal. kyr BP (McCarthy, 2011). This initiation of the WGC onto the Uummannaq shelf is later than northwest Greenland and Baffin Bay (Levac et al., 2001, Knudsen et al., 2008). This maybe a partial result of excess meltwater flux from the GIS as it retreated from the outer shelf (McCarthy, 2011). This would have diluted and cooled the basal water mass, or diverted the warm WGC water offshore (McCarthy, 2011). It is therefore unlikely that this stage of early deglaciation was triggered by the influx of warm water. Once retreat was underway, increased water depths of >600 m through the Uummannaq Trough would have led to increased ice discharge, and rapid thinning and retreat (Schoof, 2007). Enhancement of retreat rates by deep subglacial troughs is common, and has been reported in other studies from continental fjord margins (e.g. Briner et al., 2009).

Once the UISS reached the southern coast of Ubekendt Ejland, the lateral confinement within the trough increased and the bed shallowed (Figure 13b). The topographic confinement is likely to have increased lateral resistive stresses, thickening the ice and increasing basal drag. This would have reduced ice flux and caused temporary slowdown between Nuussuaq and Ubekendt Ejland. While this is likely, the current chronology means that this hypothesis cannot be further tested at present.

5.2.2. Ubekendt Ejland to the fjord margins

Once ice retreated beyond south-eastern Ubekendt Ejland the north and south regions of the UISS separated, retreating north through Igdlorssuit Sund and east towards Uummannaq respectively. The timing of retreat through Igdlorssuit Sund is constrained by ages of 12.4 kyr on southern Ubekendt Ejland (122–233 m a.s.l.) (Roberts et al., 2013) and 11.7 kyr on Karrat Island. The ages are within 2σ errors, suggesting deglaciation could have been rapid, retreating ~65 km in 0.7 kyr. Though rapid, the lateral moraine staircase on western Qeqertarssuaq suggests a coupled top-down thinning and calving during this stage of deglaciation.

This period of deglaciation (12.4-11.7 kyr) occurs during the latter part of Greenland Stadial 1 (GS1 12.9 kyr to 11.7 kyr), and the early Holocene (Lowe et al., 2008) (Figure 14), and is characterised by an increase in air temperature (~4 ‰ $\delta^{18}O$ increase in the GRIP and NGRIP record) and a regional peak in relative sea-level at ~12 kyr (Simpson et al., 2009). In conjunction with the ice margin entering the deep (500 – 600 m b.s.l.) Igdlorssuit Sund (Figures 1 and 13b and 13d), this would have acted to enhance rapid retreat back to the fjord margins. The timing of retreat from Ubekendt Ejland to the fjord margins is similar between the northern and southern sectors of the UISS, occurring by 11.5 – 10.8 kyr (Roberts et al., 2013).

5.2.3. Outer fjord to present ice margin

Following deglaciation through Igdlorssuit Sund the northern UISS progressively 'unzipped' as individual outlet glaciers retreated into their fjords. Dates from Rink-Karrat fjord suggest rapid retreat and thinning of ice across Karrat Island, with the exposure of Karrat Lake by ~11.2 cal. kyr BP, during a period of increasing air temperature (Figure 14). Following retreat to the present outer Rink-Karrat Fjord margin, geochronological data suggest that the ice margin underwent a dramatic decrease in retreat rate and temporary stagnation on east Karrat between ~11.2 and 6.9 kyr (Figure 13c). The chronological data are supported by moraines on Karrat and Nuugaatsiaq (moraines K1-3 (Figure 10) and N1-3 (Figure 8a)), providing

geomorphological evidence that retreat through Karrat Fjord was punctuated by a still-stand or re-advance.

Chronological results for moraine formation on Karrat constrain K3-N3 to 9.1 - 6.9 kyr. Dates between K3 and K1 are within errors of one another (6.5±0.5 kyr and 6.9±0.5 kyr), and suggest deposition of the moraine system by ~6.9 kyr. The similar, sub-parallel geomorphology and closely nested pattern of the moraines on Karrat Island suggest that they were not formed by a series of separate readvances. No evidence for a readvance was noted in the field, such as a second period of minerogenic input within the lake sediment cores, and an absence of bulldozed sediment within, or between, the moraines. As a result, the Karrat-Nuugaatsiaq moraine system is interpreted as forming during retreat across Karrat, punctuated by a marginal stabilisation. Similar latero-terminal moraines systems in other outer fjord localities have been identified throughout western Greenland, termed the 'Fjord Stade moraines' (Weidick, 1968, Tenbrink and Weidick, 1974, Funder, 1989, Long and Roberts, 2002, Briner et al., 2010, Young et al., 2011a, 2013a). These moraines are cited as forming as an ice sheet margin response to the GH-9.3 and GH-8.2 climatic events (Long and Roberts, 2002, Young et al., 2011a, 2013a, Briner et al., 2010). However, despite their widespread correlation with these climatic events, it has also been acknowledged that moraine formation could also be a dynamic response to, or enhanced by, topography, as ice retreated onshore (Funder, 1989, Warren and Hulton, 1990, Long et al., 2006).

Other moraine systems from West Greenland include the Umivit-Keglen, and Ørkendalen moraines, dated to 8.4-7.4 cal. kyr BP and 7.0-6.4 cal. kyr BP respectively (recalibrated dates using Calib, and IntCal09 (Reimer et al., 2011)()) (Van Tatenhove and van der Meer, 1995, van Tatenhove et al., 1996). These moraines are also thought to relate to localised marginal re-advance, induced by short periods of climatic deterioration (Tenbrink and Weidick, 1974). Within the Uummannaq region dates constrain the deposition of the Karrat-Nuugaatsiaq moraine system to between 9.1 and 6.9 kyr, therefore encompassing the period of Fjord Stade and Umivit-Keglen, /Ørkendalen moraine deposition (Long et al., 2006, Briner et al., 2010, Young et al., 2011a, Young et al., 2011b, Young et al., 2013a). This makes direct correlation with any climatic events or other moraine systems problematic when based upon fjord position and chronology alone.

The marginal still-stand observed in Rink-Karrat Fjord occurred from the onset of the Early Holocene through to the Holocene Thermal Maximum (HTM), a period from 11 to 5 kyr, characterised by a warm climate (Wanner, 2008, Jansen, 2007, Renssen et al., 2009, Kaufman et

al., 2004), Within Greenland, the HTM was characterised by temperatures 2-3°C warmer than present, suppressed precipitation levels (Anderson and Leng, 2004, Bennike et al., 2010, Axford et al., 2013), a peak in summer insolation and a drop in sea-level (Figure 14) (Long et al., 1999, Simpson et al., 2009). Though broadly constrained to 11-5 kyr, ocean-atmosphere-vegetation models have predicted that warming across central Greenland would have been greatest at 6-5 kyr (Renssen et al., 2009), Palaeoecological data from the Kangerlussuaq (Anderson and Leng, 2004, Bennike et al., 2010) and Jakobshavn (Axford et al., 2013) regions report periods of maximum warmth at 7.2-5.6 kyr and 6-4 kyr respectively.

In order to constrain the precise timing of maximum Holocene warmth in the Uummannaq region a local palaeoenvironmental reconstruction would be required, however broad chronological agreement with other areas of West Greenland would be expected. It therefore appears likely that the margin stagnation within Rink-Karrat Fjord was maintained through a period of warm climate, not conducive to ice margin stabilisation. Thus, the still-stand is hypothesised to have been controlled by non-climatic factors. Palaeo-ice stream channel width close to Karrat Island reduces to ~5 km, and bed topography shallows to ~400 m. As deeper topography exists to the east (>1000 m) and west (~700 m) of Karrat Island, this makes the area a prominent bathymetric high (Figure 14). This is most pronounced directly offshore of the Karrat-Nuugaatsiaq moraines, where a narrow topographic high occurs, displaying steep up and downstream slopes. The shallowing of the bed would have reduced the relative magnitude of ice flux necessary to maintain a stable grounding line (Jamieson et al., 2012, Schoof, 2007, Mercer, 1961). Additionally, the narrowing of the channel would have reduced the flux through increased lateral resistance (Mercer, 1961, Whillans and Van der Veen, 1997) and up-ice surface profile steepening (Jamieson et al., 2012). These topographic effects would have been sufficient to reduce calving rates and subsequently retreat rates. As a result, it appears likely that topographic constriction and shallowing facilitated the pinning of the ice margin during retreat. Such topographically controlled retreat dynamics have been reported elsewhere in Greenland (Warren and Hulton, 1990) and for Alaskan tidewater glaciers (O'Neel et al., 2005), and modelled for ice streams in Antarctica (Jamieson et al., 2012).

After the still-stand on Karrat Island, ice retreat resumed at ~6.9 kyr, reaching the spur between Rink and Umiámáko Fjords by 6.5 kyr. Here, Rink and Umiámáko Isbræ separated, their detachment evidenced by lateral moraines on the spur between the fjords (Figure 5). Following this, retreat in Rink Fjord continued, reaching ~15 km from the present ice margin by 5 kyr. The factors forcing of this final retreat from Karrat Island to Rink Isbræ's present margin (~6.9 – 5.0 kyr) are unknown, but it is likely to have been the persistence of warm air temperatures

and the influx of the warm WGC into the Uummannaq region (McCarthy, 2011). The incursion of the WGC into the Uummannaq Trough is thought to have occurred by ~8.0 kyr; however the timing of its occurrence in Rink-Karrat Fjord (and therefore its impact upon the ice margin) is unknown. The perturbation by the influx of warm water is likely to have been sufficient to detach the ice margin from its topographic pinning point at Karrat Island and force retreat into the over-deepened inner Rink Fjord and then to, or beyond, the present ice margin.

Retreat chronology in Ingia Fjord's is limited to a single date from south-east Svartenhuk, close to the fjord mouth (10.7cal. kyr BP - Bennike, 2000), and a date from Ingia peninsula (9.9 cal. kyr BP - this study). As such, it is difficult to constrain retreat through Ingia Fjord in detail, other than that ice had retreated beyond a mid-fjord position by 9.9 cal. kyr BP.

5.3. Implications for LGM ice stream history of the West Greenland Ice Sheet

Results from the Greenlandic continental shelf have provided extensive evidence for the asynchronous onset of ice stream deglaciation throughout Greenland (Evans et al., 2009, Funder et al., 2011, Ó Cofaigh et al., 2013b). This asynchronous behaviour continued through deglaciation, and is mirrored within individual outlet glaciers in the Uummannaq region. As with other GIS ice streams, the retreat of the northern UISS from its shelf-edge terminus to its present margin was driven by climatic, oceanic, and topographic forcings. Once within the inner fjord, the retreat behaviour was, however, strongly affected by channel topography and both bed depth and fjord width were the dominant control upon the rate of deglaciation. Similarly, a strong topographic control upon ice stream retreat is reported from the inner fjords of the southern UISS. Here, an ice margin stabilisation occurred in a similar topographically constricted inner fjord position as on Karrat Island. However, TCN dates from the southern UISS constrain the marginal pinning to between 11.4-9.3 kyr, again in a location characterised by channel narrowing and a shallowing in bed depth (Roberts et al., 2013). This provides further evidence for the importance of topography on glacier retreat, and exemplifies the strongly asynchronous response of outlet glaciers within the onset zone of a single ice stream system.

Also critical within the context of GIS deglacial history is the behaviour of the Karrat-Rink outlet system through the HTM to Neoglacial transition. During the early Holocene, a number of studies have demonstrated that ice was experiencing continued rapid retreat from its LGM margin (Corbett et al., 2011, Larsen et al., 2011, Hughes et al., 2012, Larsen et al.). The HTM was characterised by high air temperatures and extensive moisture starvation across the GIS.

Research has shown that this peak in air temperatures was accompanied by the widespread retreat of the GIS to an position behind its present margin between ~ 9 -7 kyr (Weidick et al., 1990, Weidick and Bennike, 2007, Roberts et al., 2010, Briner et al., 2010, Young et al., 2011b). Though broadly unknown, some have speculated that this position for Jakobshavn Isbræ was >10 km inland of the present margin (Weidick et al., 1990; Briner et al., 2010). Store Gletscher, the main outlet glacier of the southern UISS, reached its present margin by 8.7 kyr (Roberts et al., 2013), Jakobshavn Isbræ by 7 kyr (Long and Roberts, 2003, Young et al., 2011b), and in central West Greenland the Umivit-Keglen and Ørkendalen moraines suggest ice had retreated to (or beyond) its present margin occurred by 7.8 – 6.8 cal. kyr BP (Kelly, 1985). Thus, the hypothesised retreat of Rink Isbræ to a position at or beyond its present margin only after 5 kyr is much later than the deglaciation of most other ice streams in West Greenland. The Rink Isbræ margin was able to remain in a mid-fjord position throughout the HTM, displaying only a moderate retreat in response to air temperature increase. Furthermore, retreat to the present ice margin after 5.0 kyr appears to have occurred during the onset of the cold Neoglacial period (~4 kyr). This is atypical of most Greenland marine outlet glaciers/ice streams and clearly demonstrates that despite a return to a positive mass balance regime during the Neoglacial the behaviour of individual catchments and outlet systems was heavily influenced by local topographic controls on ice marginal dynamics.

6. Conclusion

The UISS existed as a large cross-shelf ice stream formed from multiple, confluent, outlet glaciers that terminated at the shelf-edge during the LGM. During the last glacial cycle, outlet glaciers in the northern Uummannaq region advanced through their fjord confines and coalesced. Geomorphological and geochronological data provide evidence for warm-based ice between 1400 and 1900 m a.s.l. in the northern UISS during the last glacial cycle. These ice thicknesses are comparable to those in the southern UISS. High altitude terrain in the north of the region forced ice to remain topographically confined within fjords, with intervening high-level areas remaining ice free, or becoming covered by cold-based ice fields. Once coalescent, ice was forced south, to the east of Ubekendt Ejland. Here it became confluent with ice from the southern UISS, draining west to the continental shelf edge. Deglaciation following the LGM took place in three stages: (1) Deglaciation from the shelf was underway by 14.9 cal. kyr BP, reaching the southeast of Ubekendt Ejland by ~12.4 kyr BP; (2) Retreat through the confluence zone was accompanied by progressive separation of the individual outlet glaciers. Retreat was rapid, and enhanced by fjord bathymetry, with ice reaching the northern outer fjords by 11.6 kyr; (3)

Retreat through the present fjord system was interrupted by a period of topographically-controlled ice marginal stabilisation between ~9.1 and 6.9 kyr.

The first two stages of retreat were synchronous between the north and south of the UISS. This retreat was controlled by climatic and oceanographic forcings, enhanced by bathymetric depths. Once within fjord confines, topographic constrictions became the dominant control upon individual outlet glacier dynamics, overriding climatic forcings, and causing early- to mid-Holocene ice marginal stabilisation in Rink-Karrat Fjord. A similar topographically controlled stabilisation occurred in the southern UISS; with a shorter duration still stand (11-9.3 kyr). Topographic control forced the northern UISS to remain on Karrat Island until 6.9 kyr, during the onset of the Holocene Thermal Maximum. Following this, Rink Isbræ retreated to a position at or beyond its present margin after 5.0 kyr. The ice within Rink-Karrat Fjord appears to have responded asynchronously with other West Greenland ice streams. Additionally, ice retreat was clearly not responding in phase with the warm HTM and cooler Neoglacial. This ice stream therefore displays a unique dynamic signal within Greenland and provides compelling evidence for a first order topographical control on ice margin stabilisation in West Greenland. It also has major implications for our understanding and reconstructions of Mid-Holocene ice sheet extent and Greenland Ice Sheet dynamics during the Neoglacial.

Acknowledgements

This work was supported by the Department of Geography (Durham University), the Department of Geography and the Environment (University of Aberdeen), the RGS-IBG, NERC CIAF Grant No: 9106/0411, and NERC Radiocarbon Facility Grant No: 1559.0411. Much of the sampling would have been impossible with the helicopter support offered by Alun Hubbard. Thanks to Arne Neumann, Birte Ørum, Barbara Stroem-Baris for logistical support, and to NERC CIAF and NERC Radiocarbon Facility staff for the preparation of cosmogenic and radiocarbon samples.

References

ANDERSON, N. J. & LENG, M. J. 2004. Increased aridity during the early Holocene in West Greenland inferred from stable isotopes in laminated-lake sediments. *Quaternary Science Reviews,* 23**,** 841-849.

AXFORD, Y., LOSEE, S., BRINER, J. P., FRANCIS, D. R., LANGDON, P. G. & WALKER, I. R. 2013. Holocene temperature history at the western Greenland Ice Sheet margin reconstructed from lake sediments. *Quaternary Science Reviews,* 59**,** 87-100.

BALCO, G., BRINER, J., FINKEL, R. C., RAYBURN, J. A., RIDGE, J. C. & SCHAEFER, J. M. 2009. Regional beryllium-10 production rate calibration for late-glacial northeastern North America. *Quaternary Geochronology,* 4**,** 93-107.

BALCO, G., STONE, J. O., LIFTON, N. A. & DUNAI, T. J. 2008. A complete and easily accessible means of calculating surface exposure ages or erosion rates from 10Be and 26739 Al measurements. *Quaternary Geochronology,* 3**,** 22.

BALLANTYNE, C. K., SCHNABEL, C. & XU, S. 2009. Exposure dating and reinterpretation of coarse debris accumulations ('rock glaciers') in the Cairngorm Mountains, Scotland. *Journal of Quaternary Science,* 24**,** 19-31.

BAMBER, J. L., LAYBERRY, R. L. & GOGINENI, S. P. 2001. A new ice thickness and bed data set for the Greenland ice sheet 1. Measurement, data reduction, and errors. *J. Geophys. Res.,* 106**,** 33773-33780.

BENNIKE, O. 2000. Palaeoecological studies of Holocene lake sediments from west Greenland. *Palaeogeography, Palaeoclimatology, Palaeoecology,* 155**,** 285-304.

BENNIKE, O., ANDERSON, N. J. & MCGOWAN, S. 2010. Holocene palaeoecology of southwest Greenland inferred from macrofossils in sediments of an oligosaline lake. *Journal of Paleolimnology,* 43**,** 787-798.

BENNIKE, O. & BJORCK, S. 2002. Chronology of the last recession of the Greenland Ice Sheet. *Journal of Quaternary Science,* 17**,** 211-219.

BONOW, J. M., LIDMAR-BERGSTRÖM, K., JAPSEN, P., CHALMERS, J. A. & GREEN, P. F. 2007. Elevated erosion surfaces in central West Greenland and southern Norway: their significance in integrated studies of passive margin development. *Norwegian Journal of Geology,* 87**,** 197-206.

BRINER, J. P., BINI, A. C. & ANDERSON, R. S. 2009. Rapid early Holocene retreat of a Laurentide outlet glacier through an Arctic fjord. *Nature Geoscience,* 2**,** 496-499.

BRINER, J. P., STEWART, H. A. M., YOUNG, N. E., PHILIPPS, W. & LOSEE, S. 2010. Using proglacial-threshold lakes to constrain fluctuations of the Jakobshavn Isbræ ice margin, western Greenland, during the Holocene. *Quaternary Science Reviews,* 29**,** 3861-3874.

BRONK RAMSEY, C. 2008. Deposition models for chronological records. *Quaternary Science Reviews,* 27**,** 42-60.

BRONK RAMSEY, C. 2009. Bayesian Analysis of Radiocarbon Dates. *Radiocarbon,* 51**,** 337-360.

CHIVERRELL, R. C., THRASHER, I. M., THOMAS, G. S. P., LANG, A., SCOURSE, J. D., VAN LANDEGHEM, K. J. J., MCCARROLL, D., CLARK, C. D., COFAIGH, C. Ó., EVANS, D. J. A. & BALLANTYNE, C. K. 2013. Bayesian modelling the retreat of the Irish Sea Ice Stream. *Journal of Quaternary Science,* 28**,** 200-209.

CORBETT, L. B., YOUNG, N. E., BIERMAN, P. R., BRINER, J. P., NEUMANN, T. A., ROOD, D. H. & GRALY, J. A. 2011. Paired bedrock and boulder< sup> 10</sup> Be concentrations resulting from early Holocene ice retreat near Jakobshavn Isfjord, western Greenland. *Quaternary Science Reviews,* 30**,** 1739-1749.

DAM, G., NØHR-HANSEN, H., PEDERSEN, G. K. & SØNDERHOLM, M. 2000. Sedimentary and structural evidence of a new early Campanian rift phase in the Nuussuaq Basin, West Greenland. *Cretaceous Research,* 21**,** 127-154.

DOWDESWELL, J. A., EVANS, J. & Ó COFAIGH, C. 2010. Submarine landforms and shallow acoustic stratigraphy of a 400 km-long fjord-shelf-slope transect, Kangerlussuaq margin, East Greenland. *Quaternary Science Reviews,* 29**,** 3359-3369.

DUNAI, T. J. & STUART, F. M. 2009. Reporting of cosmogenic nuclide data for exposure age and erosion rate determinations. *Quaternary Geochronology,* 4**,** 437-440.

EVANS, J., Ó COFAIGH, C., DOWDESWELL, J. A. & WADHAMS, P. 2009. Marine geophysical evidence for former expansion and flow of the Greenland Ice Sheet across the north-east Greenland continental shelf. *Journal of Quaternary Science,* 24**,** 279-293.

FABEL, D., BALLANTYNE, C. K. & XU, S. 2012. Trimlines, blockfields, mountain-top erratics and the vertical dimensions of the last British–Irish Ice Sheet in NW Scotland. *Quaternary Science Reviews,* 55**,** 91-102.

FUNDER, S. 1989. Quaternary geology of the ice-free areas and adjacent shelves of Greenland. *In:* FULTON, R. J. (ed.) *Quaternary Geology of Canada and Greenland.* Geological Survey of Canada and Greenland.

FUNDER, S., KJELDSEN, K. K., KJÆR, K. H. & Ó COFAIGH, C. 2011. The Greenland Ice Sheet During the Past 300,000 Years: A Review. *In:* EHLERS, J., GIBBARD, P. L. & HUGHES, P. D. (eds.) *Quaternary Glaciations - Extent and Chronology: A Closer Look.* Oxford: Elsevier.

GARDE, A. A. & STEENFELT, A. 1999. Precambrian geology of Nuussuaq and the area north-east of Disko Bugt, West Greenland. *In:* KALSBEEK, F. (ed.) *Precambrian geology of the Disko Bugt region, West Greenland.* Copenhagen: GEUS.

GILKS, W. R., RICHARDSON, S. & SPIEGELHALTER, D. 1995. *Markov Chain Monte Carlo in practice: interdisciplinary statistics*, Chapman & Hall/CRC.

GLASSER, N. F. & WARREN, C. R. 1990. Medium Scale Landforms of Glacial Erosion in South Greenland; Process and Form *Geografiska Annaler Series a-Physical Geography,* 72**,** 5.

GOSSE, J. C. & PHILLIPS, F. M. 2001. Terrestrial in situ cosmogenic nuclides: theory and application. *Quaternary Science Reviews,* 20**,** 1475-1560.

HÅKANSSON, L., ALEXANDERSON, H., HJORT, C., MOLLER, P., BRINER, J. P., ALDAHAN, A. & POSSNERT, G. 2009. Late Pleistocene glacial history of Jameson Land, central East Greenland, derived from cosmogenic Be-10 and Al-26 exposure dating. *Boreas,* 38**,** 244-260.

HÅKANSSON, L., BRINER, J., ALEXANDERSON, H., ALDAHAN, A. & POSSNERT, G. 2007. Be-10 ages from central east Greenland constrain the extent of the Greenland ice sheet during the Last Glacial Maximum. *Quaternary Science Reviews,* 26**,** 2316-2321.

HENDERSON, G. & PULVERTAFT, T. C. R. 1987a. *Descriptive text to geological map of Greenland 1:100 000, Marmorilik 71 V.2 Agnete Syd, Nugatsiaq 71 V.2 Nord and Pangnertoˆq 72 V.2 Syd,* Copenhagen,, Geol. Survey Greenland.

HENDERSON, G. & PULVERTAFT, T. C. R. 1987b. *Geological map of Greenland, 1:100 000, Mârmorilik 71 V.2 Syd, Nûgâtsiaq 71 V.2 Nord, Pangnertôq 72 V.2 Syd. Descriptive text.,* Copenhagen, Geological Survey of Greenland.

HENRIKSEN, N., HIGGINS, A. K. & KALSBEEK, F. 2000. *Greenland from Archaean to Quaternary Descriptive text to the Geological map of Greenland,1:2 500 000,* Copenhagen, GEUS.

HOLLAND, D. M., THOMAS, R. H., DE YOUNG, B., RIBERGAARD, M. H. & LYBERTH, B. 2008. Acceleration of Jakobshavn Isbrae triggered by warm subsurface ocean waters. *Nature Geoscience,* 1**,** 659-664.

HOWAT, I. M., AHN, Y., JOUGHIN, I., VAN DEN BROEKE, M. R., LENAERTS, J. T. M. & SMITH, B. 2011. Mass balance of Greenland's three largest outlet glaciers, 2000–2010. *Geophys. Res. Lett.,* 38**,** L12501.

HOWAT, I. M., JOUGHIN, I., FAHNESTOCK, M., SMITH, B. E. & SCAMBOS, T. A. 2008. Synchronous retreat and acceleration of southeast Greenland outlet glaciers 2000-06: ice dynamics and coupling to climate. *Journal of Glaciology,* 54**,** 646-660.

HOWAT, I. M., JOUGHIN, I. & SCAMBOS, T. A. 2007. Rapid changes in ice discharge from Greenland outlet glaciers. *Science,* 315**,** 1559-1561.

HUGHES, A. L., RAINSLEY, E., MURRAY, T., FOGWILL, C. J., SCHNABEL, C. & XU, S. 2012. Rapid response of Helheim Glacier, southeast Greenland, to early Holocene climate warming. *Geology,* 40**,** 427-430.

HUYBERS, P. 2006. Early Pleistocene Glacial Cycles and the Integrated Summer Insolation Forcing. *Science,* 313**,** 508-511.

JAMIESON, S. S. R., VIELI, A., LIVINGSTONE, S. J., COFAIGH, C. O., STOKES, C., HILLENBRAND, C.-D. & DOWDESWELL, J. A. 2012. Ice-stream stability on a reverse bed slope. *Nature Geosci,* advance online publication.

JANSEN, E. 2007. Climate Change 2007: The Physical Science Basis. 4th Assessment Report IPCC. Nature Publishing Group.

JOUGHIN, I., SMITH, B. E., HOWAT, I. M., FLORICIOIU, D., ALLEY, R. B., TRUFFER, M. & FAHNESTOCK, M. 2012. Seasonal to decadal scale variations in the surface velocity of Jakobshavn Isbrae, Greenland: Observation and model-based analysis. *J. Geophys. Res.,* 117**,** F02030.

KALSBEEK, F., PULVERTAFT, T. C. R. & NUTMAN, A. P. 1998. Geochemistry, age and origin of metagreywackes from the Palaeoproterozoic Karrat Group, Rinkian Belt, West Greenland. *Precambrian Research,* 91**,** 383-399.

KAUFMAN, D. S., AGER, T. A., ANDERSON, N. J., ANDERSON, P. M., ANDREWS, J. T., BARTLEIN, P. J., BRUBAKER, L. B., COATS, L. L., CWYNAR, L. C., DUVALL, M. L., DYKE, A. S., EDWARDS, M. E., EISNER, W. R., GAJEWSKI, K., GEIRSDÓTTIR, A., HU, F. S., JENNINGS, A. E., KAPLAN, M. R., KERWIN, M. W., LOZHKIN, A. V., MACDONALD, G. M., MILLER, G. H., MOCK, C. J., OSWALD, W. W., OTTO-BLIESNER, B. L., PORINCHU, D. F., RÜHLAND, K., SMOL, J. P., STEIG, E. J. & WOLFE, B. B. 2004. Holocene thermal maximum in the western Arctic (0–180°W). *Quaternary Science Reviews,* 23**,** 529-560.

KELLY, M. 1980. *The status of the Neoglacial in western Greenland*, Grønlands geologiske undersøgelse.

KELLY, M. 1985. A review of the Quaternary geology of western Greenland. *In:* ANDREWS, J. T. (ed.) *Quaternary Environments in Eastern Canadian Arctic, Baffin Bay and Western Greenland.* Boston: Allen and Unwin.

KNUDSEN, K. L., STABELL, B., SEIDENKRANTZ, M. S., EIRIKSSON, J. & BLAKE JR, W. 2008. Deglacial and Holocene conditions in northernmost Baffin Bay: sediments, foraminifera, diatoms and stable isotopes. *Boreas,* 37**,** 346-376.

LARSEN, N. K., FUNDER, S., KJÆR, K. H., KJELDSEN, K. K., KNUDSEN, M. F. & LINGE, H. Rapid early Holocene ice retreat in West Greenland. *Quaternary Science Reviews*.

LARSEN, N. K., KJÆR, K. H., OLSEN, J., FUNDER, S., KJELDSEN, K. K. & NØRGAARD-PEDERSEN, N. 2011. Restricted impact of Holocene climate variations on the southern Greenland Ice Sheet. *Quaternary Science Reviews,* 30**,** 3171-3180.

LEVAC, E., VERNAL, A. D. & BLAKE JR, W. 2001. Sea-surface conditions in northernmost Baffin Bay during the Holocene: palynological evidence. *Journal of Quaternary Science,* 16**,** 353-363.

LONG, A. J. & ROBERTS, D. H. 2002. A revised chronology for the 'Fjord Stade' moraine in Disko Bugt, west Greenland. *Journal of Quaternary Science,* 17**,** 561-579.

LONG, A. J. & ROBERTS, D. H. 2003. Late Weichselian deglacial history of Disko Bugt, West Greenland, and the dynamics of the Jakobshavns Isbrae ice stream. *Boreas,* 32**,** 208-226.

LONG, A. J., ROBERTS, D. H. & DAWSON, S. 2006. Early Holocene history of the west Greenland Ice Sheet and the GH-8.2 event. *Quaternary Science Reviews,* 25**,** 904-922.

LONG, A. J., ROBERTS, D. H. & WRIGHT, M. R. 1999. Isolation basin stratigraphy and Holocene relative sea-level change on Arveprinsen Ejland, Disko Bugt, West Greenland. *Journal of Quaternary Science,* 14**,** 323-345.

LOWE, J. J., RASMUSSEN, S. O., BJÖRCK, S., HOEK, W. Z., STEFFENSEN, J. P., WALKER, M. J. C. & YU, Z. C. 2008. Synchronisation of palaeoenvironmental events in the North Atlantic region during the Last Termination: a revised protocol recommended by the INTIMATE group. *Quaternary Science Reviews,* 27**,** 6-17.

LYKKE-ANDERSEN, H. 1998. NEOGENE–QUATERNARY DEPOSITIONAL HISTORY OF THE EAST GREENLAND SHELF IN THE VICINITY OF LEG 152 SHELF SITES. *Proceedings of the Ocean Drilling Program, Scientific Results,* 152**,** 29-38.

MADEN, C., ANASTASI, P. A. F., DOUGANS, A., FREEMAN, S. P. H. T., KITCHEN, R., KLODY, G., SCHNABEL, C., SUNDQUIST, M., VANNER, K. & XU, S. 2007. SUERC AMS ion detection. *Nuclear Instruments and Methods in Physics Research Section B: Beam Interactions with Materials and Atoms,* 259**,** 131-139.

MCCARTHY, D. J. 2011. *Late Quaternary ice-ocean interactions in central West Greenland.* PhD, Durham University.

MERCER, J. H. 1961. The Response of Fjord Glaciers to changes in the Firn Limit. *Journal of Glaciology,* 3**,** 850-858.

NICK, F. M., VIELI, A., HOWAT, I. M. & JOUGHIN, I. 2009. Large-scale changes in Greenland outlet glacier dynamics triggered at the terminus. *Nature Geoscience,* 2**,** 110-114.

NISHIIZUMI, K., WINTERER, E. L., KOHL, C. P., KLEIN, J., MIDDLETON, R., LAL, D. & ARNOLD, J. R. 1989. Cosmic ray production rates of 10Be and 26Al in quartz from glacially polished rocks. *Journal of Geophysical Research: Solid Earth,* 94**,** 17907-17915.

O'NEEL, S., PFEFFER, W. T., KRIMMEL, R. & MEIER, M. 2005. Evolving force balance at Columbia Glacier, Alaska, during its rapid retreat. *Journal of Geophysical Research: Earth Surface,* 110**,** F03012.

Ó COFAIGH, C., ANDREWS, J. T., JENNINGS, A. E., DOWDESWELL, J. A., HOGAN, K. A., KILFEATHER, A. A. & SHELDON, C. 2013a. Glacimarine lithofacies, provenance, and depositional processes on a West Greenland trough-mouth fan. *Journal of Quaternary Science,* 28**,** 13-26.

Ó COFAIGH, C., DOWDESWELL, J., EVANS, J., KENYON, N. H., TAYLOR, J., MIENERT, J. & WILKEN, M. 2004. Timing and significance of glacially influenced mass-wasting in the submarine channels of the Greenland Basin. *Marine Geology,* 207**,** 39-54.

Ó COFAIGH, C., DOWDESWELL, J. A., JENNINGS, A. E., HOGAN, K. A., KILFEATHER, A., HIEMSTRA, J. F., NOORMETS, R., EVANS, J., MCCARTHY, D. J., ANDREWS, J. T., LLOYD, J. M. & MOROS, M. 2013b. An extensive and dynamic ice sheet on the West Greenland shelf during the last glacial cycle. *Geology,* 41**,** 219-222.

PEDERSEN, G. K. & PULVERTAFT, T. C. R. 1992. The nonmarine Cretaceous of the West Greenland Basin, onshore West Greenland. *Cretaceous Research,* 13**,** 263-272.

PUTKONEN, J. & SWANSON, T. 2003. Accuracy of cosmogenic ages for moraines. *Quaternary Research,* 59**,** 255-261.

REEH, N. 1985. Was the Greenland ice sheet thinner in the late Wisconsinan than now? *Nature,* 317**,** 797-799.

REIMER, P. J., BAILLIE, M. G. L., BARD, E., BAYLISS, A., BECK, J. W., BLACKWELL, P. G., RAMSEY, C. B., BUCK, C. E., BURR, G. S., EDWARDS, R. L., FRIEDRICH, M., GROOTES, P. M., GUILDERSON, T. P., HAJDAS, I., HEATON, T. J., HOGG, A. G., HUGHEN, K. A., KAISER, K. F., KROMER, B., MCCORMAC, F. G., MANNING, S. W., REIMER, R. W., RICHARDS, D. A., SOUTHON, J. R., TALAMO, S., TURNEY, C. S. M., VAN DER PLICHT, J. & WEYHENMEYER, C. E. 2011. *IntCal09 and Marine09 Radiocarbon Age Calibration Curves, 0-50,000 Years cal BP*.

RENSSEN, H., SEPPA, H., HEIRI, O., ROCHE, D. M., GOOSSE, H. & FICHEFET, T. 2009. The spatial and temporal complexity of the Holocene thermal maximum. *Nature Geosci,* 2**,** 411-414.

RIGNOT, E. & KANAGARATNAM, P. 2006. Changes in the velocity structure of the Greenland Ice Sheet. *Science,* 311**,** 986-990.

RIGNOT, E., VELICOGNA, I., VAN DEN BROEKE, M. R., MONAGHAN, A. & LENAERTS, J. 2011. Acceleration of the contribution of the Greenland and Antarctic ice sheets to sea level rise. *Geophys. Res. Lett.,* 38**,** L05503.

RINTERKNECHT, V., GOROKHOVICH, Y., SCHAEFER, J. & CAFFEE, M. 2009. Preliminary Be-10 chronology for the last deglaciation of the western margin of the Greenland Ice Sheet. *Journal of Quaternary Science,* 24**,** 270-278.

ROBERTS, D. H. & LONG, A. J. 2005. Streamlined bedrock terrain and fast ice flow, Jakobshavns Isbrae, West Greenland: implications for ice stream and ice sheet dynamics. *Boreas,* 34**,** 25-42.

ROBERTS, D. H., LONG, A. J., DAVIES, B. J., SIMPSON, M. J. R. & SCHNABEL, C. 2010. Ice stream influence on West Greenland Ice Sheet dynamics during the Last Glacial Maximum. *Journal of Quaternary Science,* 25**,** 850-864.

ROBERTS, D. H., LONG, A. J., SCHNABEL, C., DAVIES, B. J., XU, S., SIMPSON, M. J. R. & HUYBRECHTS, P. 2009. Ice sheet extent and early deglacial history of the southwestern sector of the Greenland Ice Sheet. *Quaternary Science Reviews,* 28**,** 2760-2773.

ROBERTS, D. H., LONG, A. J., SCHNABEL, C., FREEMAN, S. & SIMPSON, M. J. R. 2008. The deglacial history of southeast sector of the Greenland Ice Sheet during the Last Glacial Maximum. *Quaternary Science Reviews,* 27**,** 1505-1516.

ROBERTS, D. H., REA, B. R., LANE, T. P., SCHNABEL, C. & RODES, A. 2013. New constraints on Greenland ice sheet dynamics during the last glacial cycle: evidence from the Uummannaq ice stream system. *Journal of Geophysical Research (Earth Surface)*.

SCHOOF, C. 2007. Ice sheet grounding line dynamics: Steady states, stability, and hysteresis. *Journal of Geophysical Research,* 112**,** F03S28.

SIMPSON, M. J. R., MILNE, G. A., HUYBRECHTS, P. & LONG, A. J. 2009. Calibrating a glaciological model of the Greenland ice sheet from the Last Glacial Maximum to present-day using field observations of relative sea level and ice extent. *Quaternary Science Reviews,* 28**,** 1631-1657.

STOKES, C. R. & CLARK, C. D. 1999. Geomorphological criteria for identifying Pleistocene ice streams. *Annals of Glaciology,* 28**,** 67-79.

SUGDEN, D. E. 1974. Landscapes of glacial erosion in Greenland and their relationship to ice, topographic and bedrock conditions. *In:* BROWN, E. H. & WATERS, R. S. (eds.) *Progress in Geomorphology: Papers in honour of David L. Linton. Institute of British Geographers Special Publication. No. 7.* London: Institute of British Geographers.

SWIFT, D. A., PERSANO, C., STUART, F. M., GALLAGHER, K. & WHITHAM, A. 2008. A reassessment of the role of ice sheet glaciation in the long-term evolution of the East Greenland fjord region. *Geomorphology,* 97**,** 109-125.

TENBRINK, N. W. & WEIDICK, A. 1974. Greenland Ice Sheet History since Last Glaciation. *Quaternary Research,* 4**,** 429-&.

THOMAS, R., FREDERICK, E., KRABILL, W., MANIZADE, S. & MARTIN, C. 2009. Recent changes on Greenland outlet glaciers. *Journal of Glaciology,* 55**,** 147-162.

THOMAS, R., FREDERICK, E., LI, J., KRABILL, W., MANIZADE, S., PADEN, J., SONNTAG, J., SWIFT, R. & YUNGEL, J. 2011. Accelerating ice loss from the fastest Greenland and Antarctic glaciers. *Geophys. Res. Lett.,* 38**,** L10502.

THOMAS, R. H. 2004. Force-perturbation analysis of recent thinning and acceleration of Jakobshavn Isbrae, Greenland. *Journal of Glaciology,* 50**,** 57-66.

VAN TATENHOVE, F. G. M. & VAN DER MEER, J. J. M. 1995. Glacial-Geological/Geomorphological Research in West Greenland used to test an Ice-Sheet model. *Quaternary Research,* 44**,** 317-327.

VAN TATENHOVE, F. G. M., VAN DER MEER, J. J. M. & KOSTER, E. A. 1996. Implications for Deglaciation Chronology from New AMS Age Determinations in Central West Greenland. *Quaternary Research,* 45**,** 245-253.

VELICOGNA, I. & WAHR, J. 2006. Acceleration of Greenland ice mass loss in spring 2004. *Nature,* 443**,** 329-331.

VIELI, A. & NICK, F. 2011. Understanding and Modelling Rapid Dynamic Changes of Tidewater Outlet Glaciers: Issues and Implications. *Surveys in Geophysics,* 32**,** 437-458.

WANNER, H. 2008. Mid- to late Holocene climate change: An overview. *Quat. Sci. Rev.,* 27**,** 1791-1828.

WARREN, C. R. & HULTON, N. R. J. 1990. Topographic and glaciological controls on Holocene ice-sheet margin dynamics, central West Greenland. *Annals of Glaciology,* 14**,** 307-310.

WEIDICK, A. 1968. Observations on some Holocene glacier fluctuations in west Greenland. *Meddelelsser om Grønland,* 165.

WEIDICK, A. & BENNIKE, O. 2007. Quaternary glaciation history and glaciology of Jakobshavn Isbrae and the Disko Bugt region, West Greenland: A review. *Geological Survey of Denmark and Greenland Bulletin,* 14**,** 1-78.

WEIDICK, A., OERTER, H., REEH, N., THOMSEN, H. H. & THORNING, L. 1990. The Recession of the Inland Ice Margin during the Holocene Climatic Optimum in the Jakobshavn-Isfjord Area of West Greenland. *Global and Planetary Change,* 8**2,** 389-399.

WHILLANS, I. M. & VAN DER VEEN, C. J. 1997. The role of lateral drag in the dynamics of Ice Stream B,Antarctica. *Journal of Glaciology,* 43**,** 231-237.

WILSON, P., BENTLEY, M. J., SCHNABEL, C., CLARK, R. & XU, S. 2008. Stone run (block stream) formation in the Falkland Islands over several cold stages, deduced from cosmogenic isotope (10Be and 26Al) surface exposure dating. *Journal of Quaternary Science,* 23**,** 461-473.

WOLFE, A. P., MILLER, G. H., OLSEN, C. A., FORMAN, S. L., DORAN, P. T. & HOLMGREN, S. U. 2004. Geochronology of high latitude lake sediments. *In:* PIENITZ, R., DOUGLAS, M. S. & SMOL, J. P. (eds.) *Long-term environmental change in Arctic and Antarctic lakes.* Springer.

YOUNG, N. E., BRINER, J., ROOD, D., FINK, D., CORBETT, L. B. & BIERMAN, P. 2013a. Age of the Fjord Stade moraines in the Disko Bugt region, western Greenland, and the 9.3 and 8.2 ka cooling events. *Quaternary Science Reviews,* 60**,** 76-90.

YOUNG, N. E., BRINER, J. P., AXFORD, Y., CSATHO, B., BABONIS, G. S., ROOD, D. H. & FINKEL, R. C. 2011a. Response of a marine-terminating Greenland outlet glacier to abrupt cooling 8200 and 9300 years ago. *Geophys. Res. Lett.,* 38**,** L24701.

YOUNG, N. E., BRINER, J. P., STEWART, H. A. M., AXFORD, Y., CSATHOS, B., ROOD, D. H. & FINKEL, R. C. 2011b. Response of Jakobshavn Isbræ, Greenland, to Holocene climate change. *Geology,* 39**,** 131-145.

YOUNG, N. E., SCHAEFER, J. M., BRINER, J. P. & GOEHRING, B. M. 2013b. A 10Be production-rate calibration for the Arctic. *Journal of Quaternary Science,* 28**,** 515-526.

Table 1. Fjord locations, characteristics and outlet glacier ice flux throughout the Uummannaq region. Outlet glacier locations are identified in Figure 1

Fjord Name	Mouth location	Snout location	Orient (°)	Length (km)	Width at SL (km)	Plateau height (m a.s.l)	Max. water depth (m)[a]	Max ice flux ($km^3\ yr^{-1}$)[b]
Northern Fjords								
Ingia Fjord	71.73°N 53.32°W	72.00°N 52.70°W	213.4	38.5	4.5	1444	-	1.1
Rink-Karrat Fjord	71.40°N 53.07°W	71.73°N 53.65°W	238.1	63.6	6.2	1791	1108	11.8
Kangerdlugssuaq	71.38°N 53.00°W	71.45°N 51.83°W	263.2	61.7	4.2	1894	570	2.4
Southern Fjords								
Kangerdluarssuk	71.13°N 52.30°W	71.25°N 51.52°W	245	34.9	5.7	1671	770	0.3
Perdlerjiup Kangerdlua	71.05°N 52.00°W	70.98°N 50.95°W	282	42.5	5.5	1388	1246	1
Itivdliarssup Kangerdlua	70.98°N 51.97°W	70.80°N 51.00°W	302.1	42.5	5.6	1332	844	7.6
Sermigdlip Kangerdlua	70.7°N 51.52°W	70.62°N 50.63°W	291.5	38.2	4.4	1180	1287	2.6
Qarajaqs Isfjord	70.68°N 52.28°W	70.37°N 50.60°W	302.7	75.4	6.9	1308	956	17.8

[a]Data from GEBCO_08 Grid and Hareø-Prøven bathymetric charts
[b]Data from (Bauer et al., 1968; Carbonnell and Bauer, 1968; Rignot and Kanagaratnam, 2006b)

Table 2. TCN sample locations, elevations, type and shielding factors for samples presented in this study.

Sample code	Latitude (°N)	Longitude (°W)	Elevation (m a.s.l.)	Sample type	Thickness (cm)[a]	Sample density (g/cm^3)	Shielding factor
KA2	71.483	53.126	720	Bedrock	5	2.6	0.9949
KA3	71.654	51.999	1402	Bedrock	5	2.6	0.9951
KA5	71.671	52.391	1964	Bedrock	5	2.6	1
KA6	71.518	52.943	276	Erratic	5	2.6	0.9995
KA9	71.510	53.0279	482	Bedrock	5	2.6	0.9794
KA10	71.513	53.0278	380	Bedrock	5	2.6	0.9886
KA11	71.516	53.0276	286	Bedrock	5	2.6	0.9889
KA12	71.521	52.993	160	Bedrock	5	2.6	0.99018
KA15	71.525	52.968	76	Bedrock	5	2.6	0.9910
KA16	71.529	52.880	78	Bedrock	5	2.6	0.9967
KA17	71.529	52.880	69	Erratic	5	2.6	0.9977
KA18	71.527	52.901	148	Bedrock	5	2.6	0.9989
KA19	71.527	52.906	148	Erratic	5	2.6	0.9986
KA20	71.629	52.136	400	Erratic	5	2.6	0.9699
KA21	71.630	52.137	411	Bedrock	5	2.6	0.9411
KA23	71.633	52.082	110	Bedrock	5	2.6	0.9604
KA24	71.621	52.940	1019	Bedrock	5	2.6	0.9998
KA27	71.641	52.564	162	Bedrock	5	2.6	0.9934

[a] The top faces of all samples were exposed at the surface.

Table 3. ^{10}Be TCN exposure ages from the northern UISS

Sample code	^{10}Be conc. (at g^{-1})[abc]	Muon prod. rate (at gr^{-1} yr^{-1})	Spallation prod. rate (at g^{-1} yr^{-1})	^{10}Be Exposure age (yrs)[d,e,f]	Internal uncertainty (yr)	External uncertainty (yr)
KA2	97476 ± 5258	0.236	8.09	11686	632	1198
KA3	284023 ± 13055	0.298	14.71	18932	874	1869
KA5	2119500 ± 72370	0.359	23.1	92027	3216	8789
KA6	65286 ± 2738	0.201	5.28	11939	502	763
KA9	79977 ± 3403	0.217	6.36	12146	518	1178
KA10	43476 ± 2895	0.209	5.81	7241	483	596
KA11	49532 ± 4240	0.202	5.28	9055	777	891
KA15	9606 ± 5663	0.187	4.23	2177	1284	1288
KA17	30340 ± 1485	0.187	4.22	6862	336	685
KA18	16276 ± 1287	0.192	4.61	3375	267	397
KA19	31312 ± 1805	0.192	4.61	6529	377	491
KA20	31451 ± 4156	0.210	5.84	5208	689	733
KA21	31207 ± 2191	0.211	5.7	5283	371	450
KA23	22171 ± 2271	0.189	4.26	4993	512	566
KA27	32099 ± 5073	0.193	4.66	6624	1049	1096

[a] All beryllium-10 derived from quartz

[b] Uncertainties are reported at the 1σ confidence level.

[c] Propagated uncertainties include error in the blank, carrier mass (1 per cent) and counting statistics.

[d] Calculation of ages was carried out assuming no erosion

[e] Exposure ages are based upon the constant production rate model, using the scaling scheme for spallation from Lal (1991) and Stone (2000), and the NENA calibration (Balco et al., 2009).

[f] Dates were calculated using the CRONUS-Earth online calculator, version 2.2 (Balco et al., 2008).

Table 4. ^{26}Al TCN exposure ages from the northern UISS

Sample code	^{26}Al (at g^{-1})[a,b,c]	Muon prod^{n} rate (at gr^{-1} yr^{-1})	Spall^{n} prod^{n} rate (at g^{-1} yr^{-1})	^{26}Al Exposure age (yrs)[d,e,f]	Internal uncertainty (yr)	External uncertainty (yr)	^{26}Al/^{10}Be ratios
KA2	764049 ± 125967	1.971	54.6	13536	2247	2350	7.84±1.45
KA3	2272889 ± 91694	2.496	99.23	22491	917	1433	8.00±0.69
KA5	14630123 ± 428055	3.008	155.85	96084	2948	5693	6.90±0.53
KA9	513851 ± 37179	1.81	42.9	11507	837	1009	6.42±0.70
KA10	338083 ± 34256	1.745	39.17	8297	844	934	7.78 ± 0.94
KA11	425895 ± 52326	1.686	35.63	11479	1418	1523	8.60 ± 1.29

[a] Al aluminium-26 derived from quartz

[b] Uncertainties are reported at the 1σ confidence level.

[c] Propagated uncertainties include error in the blank, carrier mass (1 per cent) and counting statistics.

[d] Calculation of ages was carried out assuming no erosion

[e] Exposure ages are based upon the constant production rate model, using the scaling scheme for spallation from Lal (1991) and Stone (2000), and the NEMA calibration (Balco et al., 2009).

[f] Dates were calculated using the CRONUS-Earth online calculator, version 2.2 (Balco et al., 2008).

Table 5. ^{14}C ages and calibrated age ranges for the two lake sites in this study. ^{14}C age is the radiocarbon age corrected for isotopic fractionation, measured and calculated using $\delta^{13}C$. Errors are quoted to 1σ. Ages were calibrated using OxCal 4.2 and the IntCal09 calibration curve, and presented as a range to 2σ.

Pub. code	Sample code	Lat. (°N)	Long (°W)	Sample type	$\delta^{13}C_{VPDB}$‰ ± 0.1	Carbon content (% by wt.)	^{14}C Age	Uncertainty 1σ (14C yrs BP)	cal. Min (yr)	cal. Max (yr)	cal. mid (yr)
SUERC-37526	InL1	71.86	53.03	Plant macros	-27.9	27.5	8811	40	9685	9954	9819.5
SUERC-37530	KaL1	71.51	52.95	Bulk lake gyttja	-19.8	4.5	9838	41	11196	11316	11256

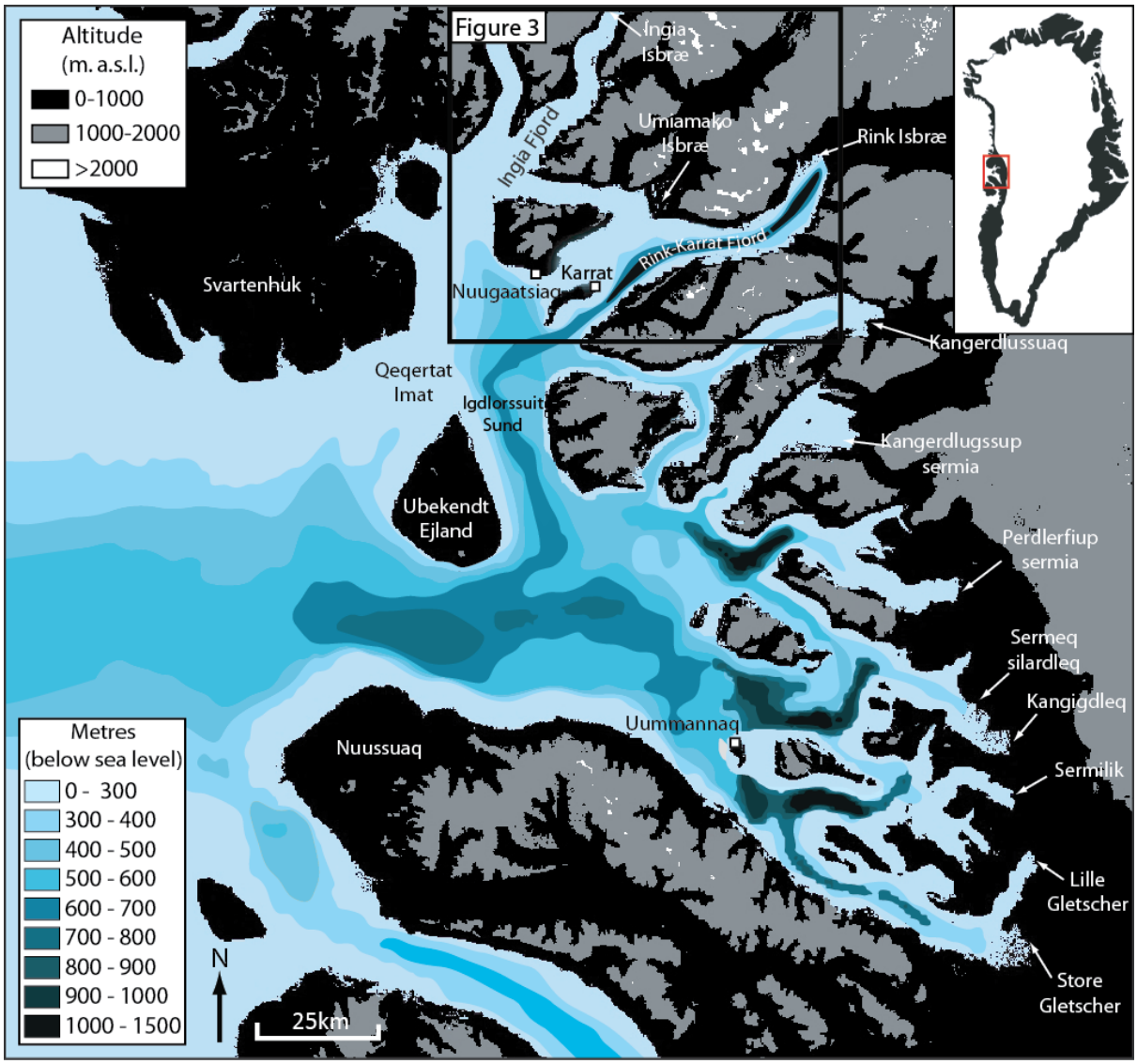

Figure 1. Topographic and bathymetric overview of the Uummannaq region, with key locations marked. Note the higher average altitude of land masses in the north of the region, and the shallow Qeqertat Imát north of Ubekendt Ejland, in comparison to the deep Uummannaq Trough. Bathymetric depths are from IBCAO data (Jakobsson et al., 2012).

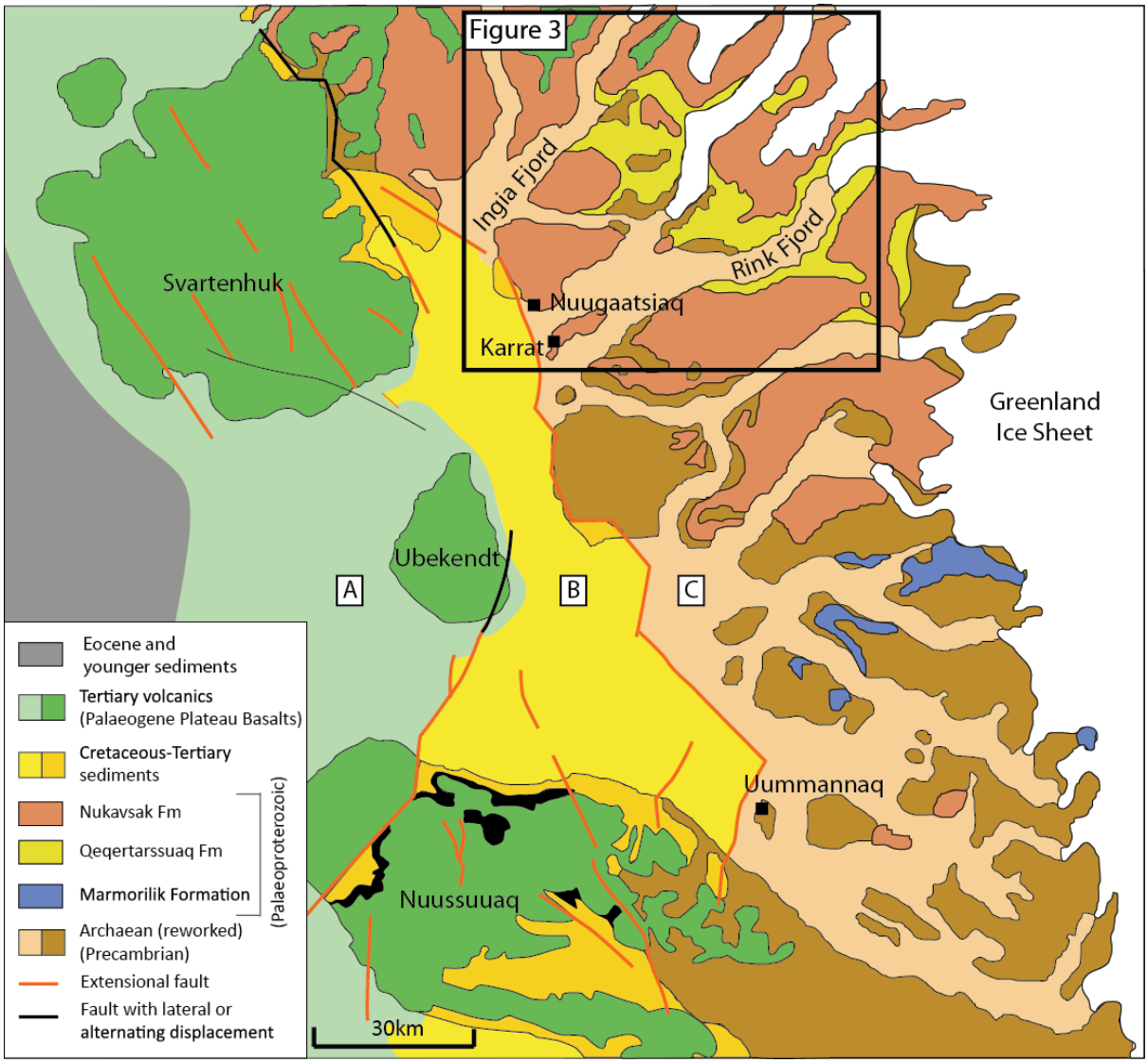

Figure 2. Map of the Uummannaq region showing dominant bedrock geology (adapted from Steenfelt et al., 1998. The three distinct geological regions (A, B, and C) can be seen, separated by north to south trending faults (adapted from Steenfelt et al., 1998).

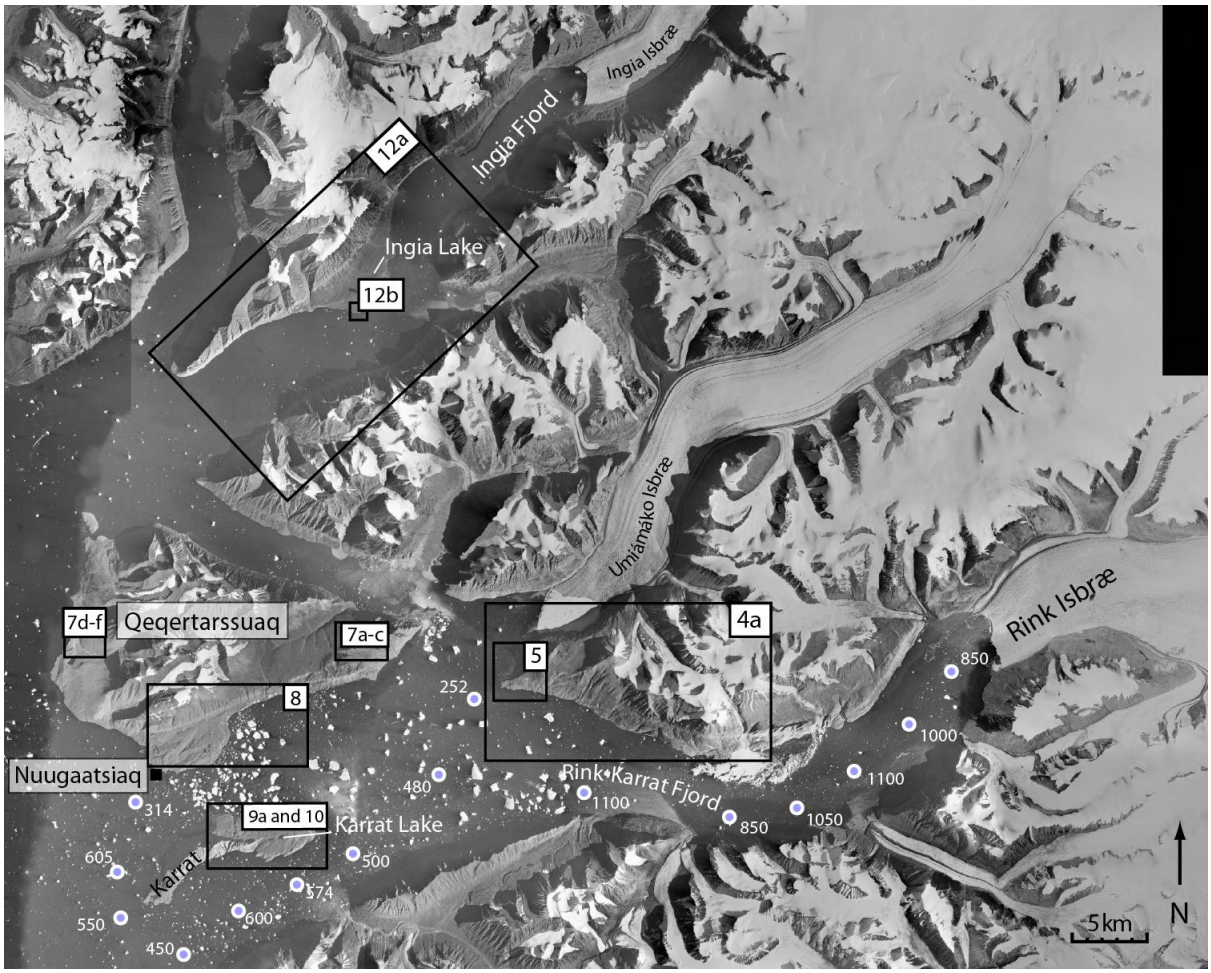

Figure 3. Aerial photograph of the study area in the northern Uummannaq region. The focus of this study was Rink – Karrat Fjord and Ingia Fjord, in the south and north of this image respectively. Boxes indicate the locations of other figures. Fjord depths are shown by blue filled circles (from Hareø-Prøven bathymetric charts).

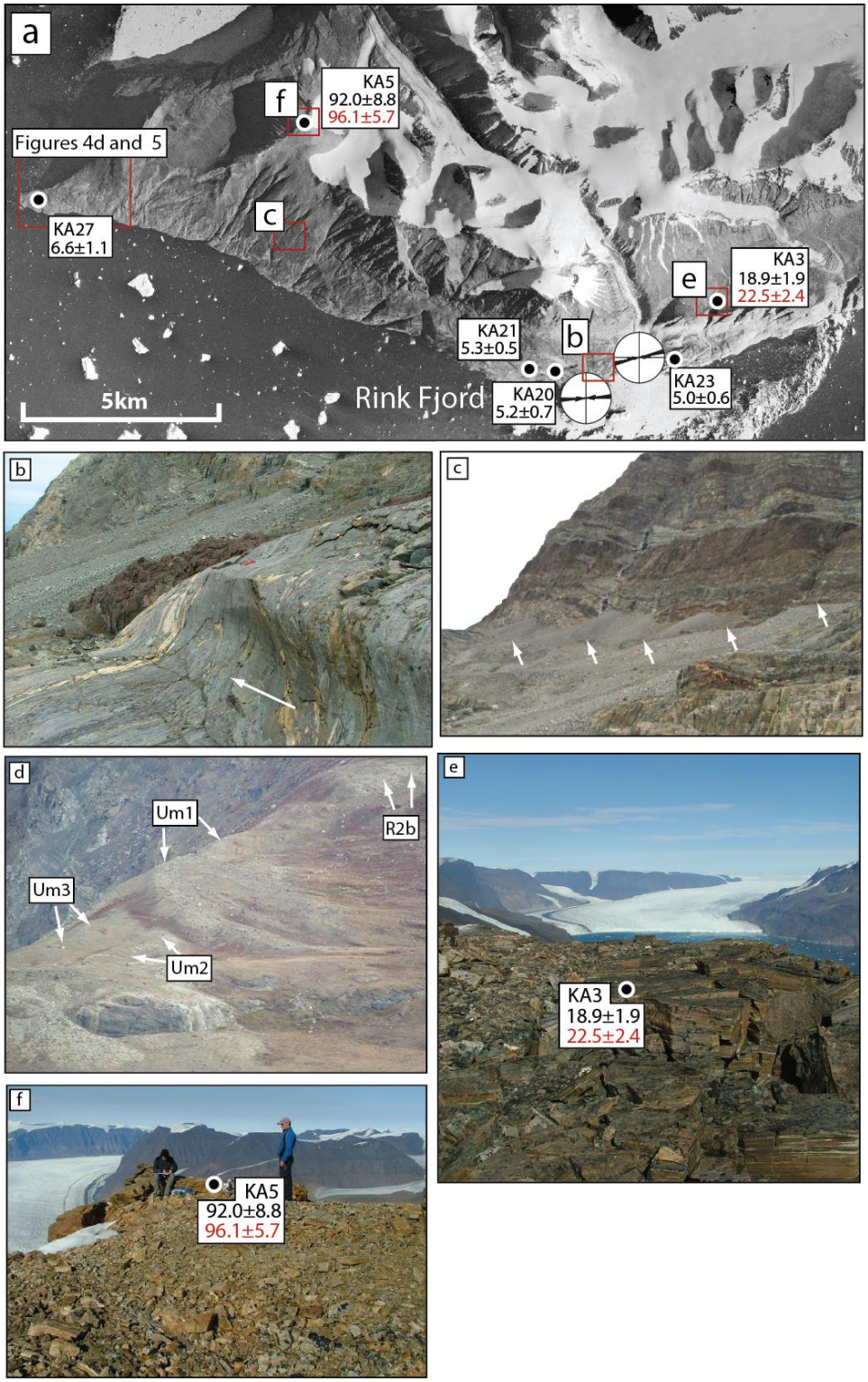

Figure 4. Plate of photographs from inner Rink-Karrat Fjord. (a) Aerial photograph showing an overview of inner Rink Fjord, with striae shown (n=50 per rose diagram) (b) Fragmentary lateral moraine at 740 m a.s.l. in inner Rink Fjord (arrowed); (c) Striated, ice moulded roche moutonnee with lateral p-form arrowed; (d) Moraines Um1-3 and R3 (all arrowed) at the Rink- Umiámáko confluence (see Figure 5 for moraine location); (e) Autochonous blockfield at 1400 m a.s.l. in inner Rink Fjord. (f) Autochonous blockfield at 1900 m a.s.l. on Pyramid Stubben.

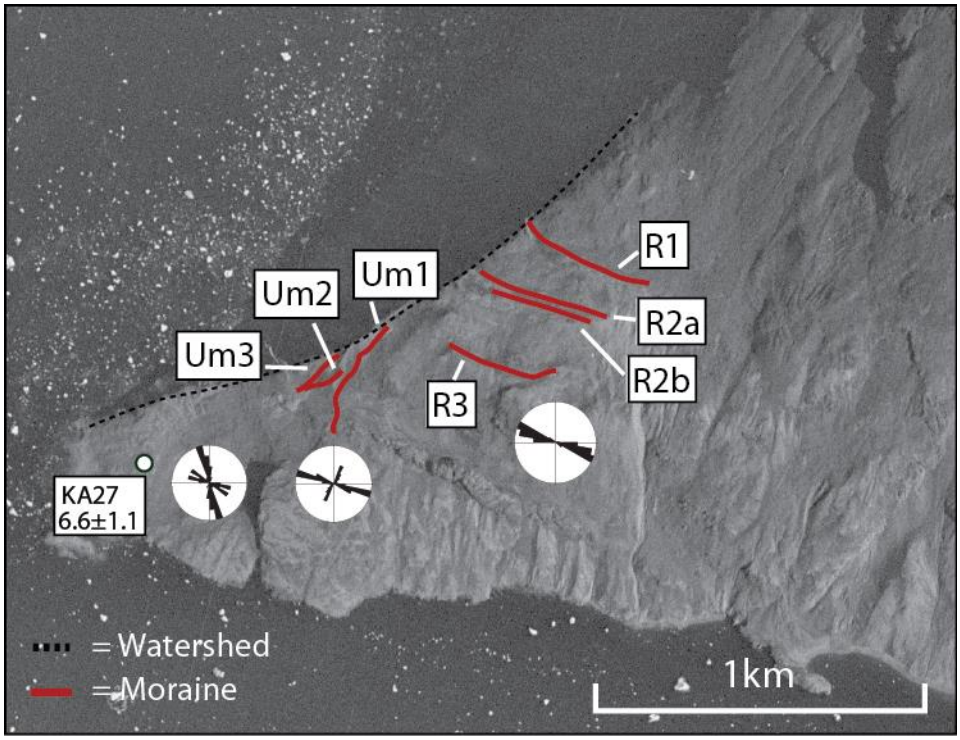

Figure 5. Aerial photograph of the spur between Rink and Umiámáko Isbræs (see Figure 4a for location). Two discrete sets of moraines were mapped in the field, with on corresponding to ice activity in Rink Fjord (R1-R3), and one to ice in Umiámáko Fjord (Um1-3).

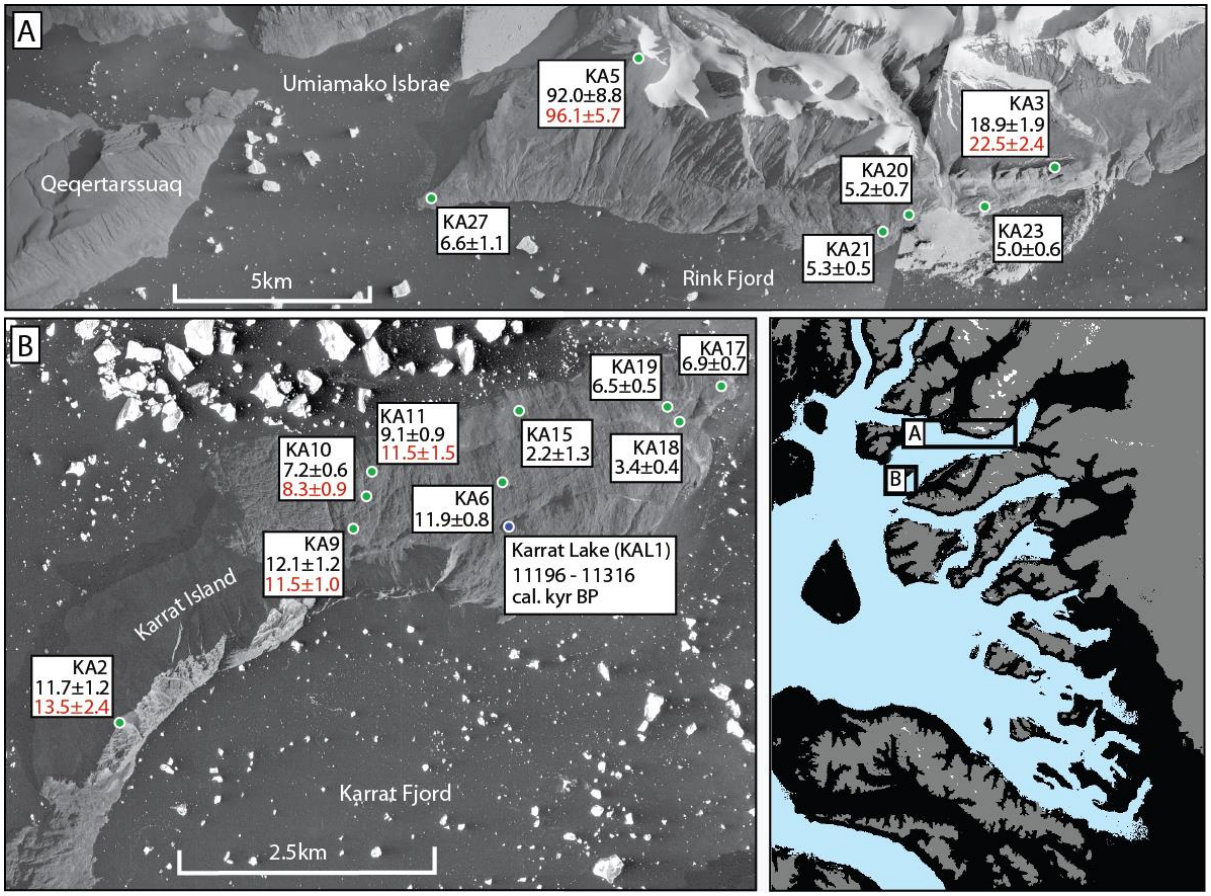

Figure 6. Aerial photographs showing the locations of samples taken for dating throughout Rink and Karrat Fjord, and their results. Successful TCN results are shown by green circles (^{10}Be ages in black, ^{26}Al ages in red). Bedrock samples have a black box, erratic boulder samples have a green box. ^{14}C result is indicated by the blue circle.

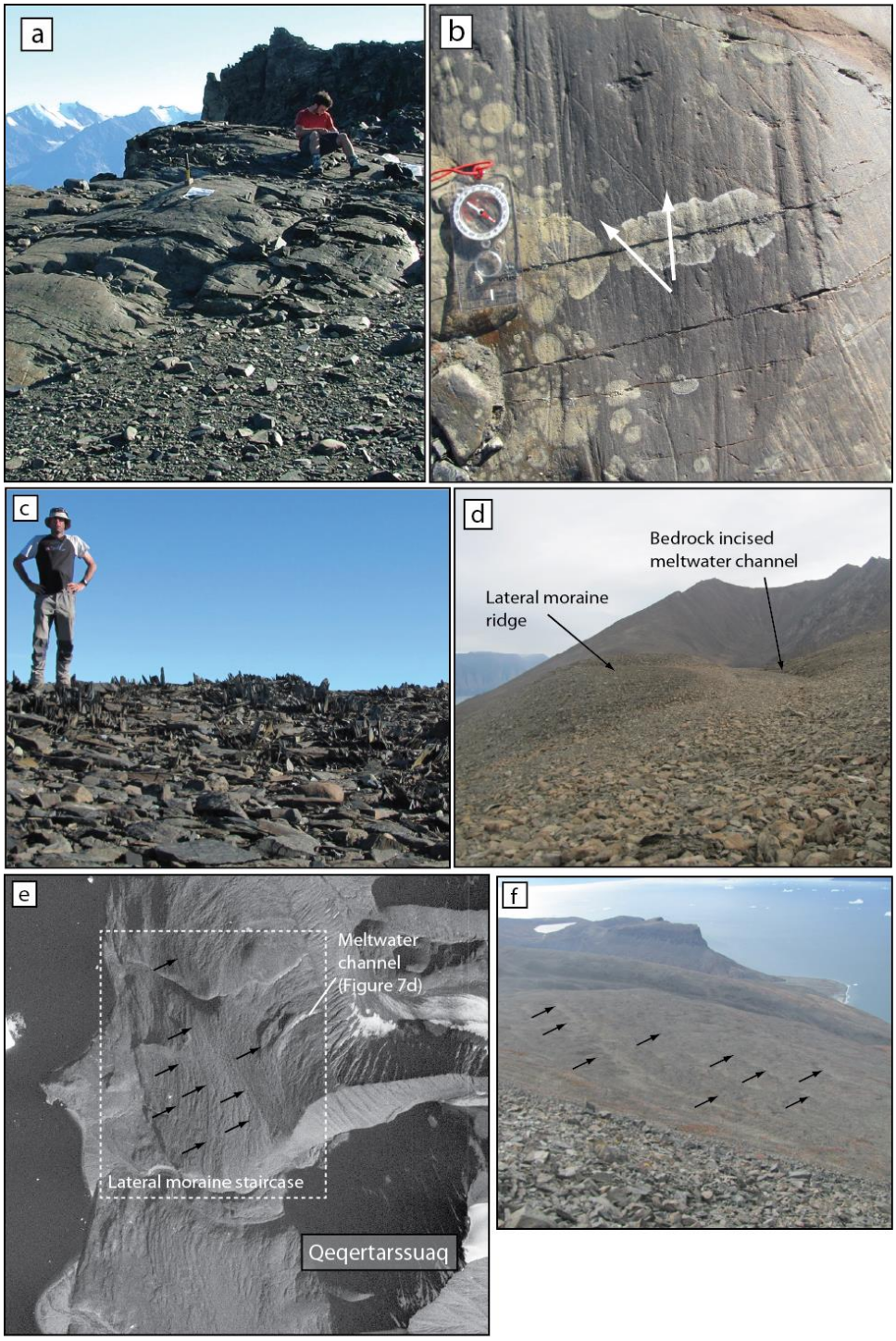

Figure 7. Plate of photographs from Qeqertarssuaq. (a) ice-moulded bedrock outcrops at 1040 m a.s.l. on eastern Qeqertarssuaq, (b) enlargement of the striated, ice moulded bedrock surface from the bedrock outcrop beside the seated person in Figure 7a, (c) frost shattered and heaved local material at ~1000 m a.s.l., eastern Qeqertarssuaq, (d) large lateral moraine (Q1– 786 m a.s.l.) on western Qeqertarssuaq, abutting a bedrock cut lateral meltwater channel. See person on moraine ridge for scale. (e) Aerial photograph of western Qeqertarssuaq, with the meltwater channel of Figure 7d labelled, and the area of lateral moraines boxed, with individual ridges arrowed. (f) Oblique photograph from close to the meltwater channel, looking southwest. Lateral moraines are arrowed.

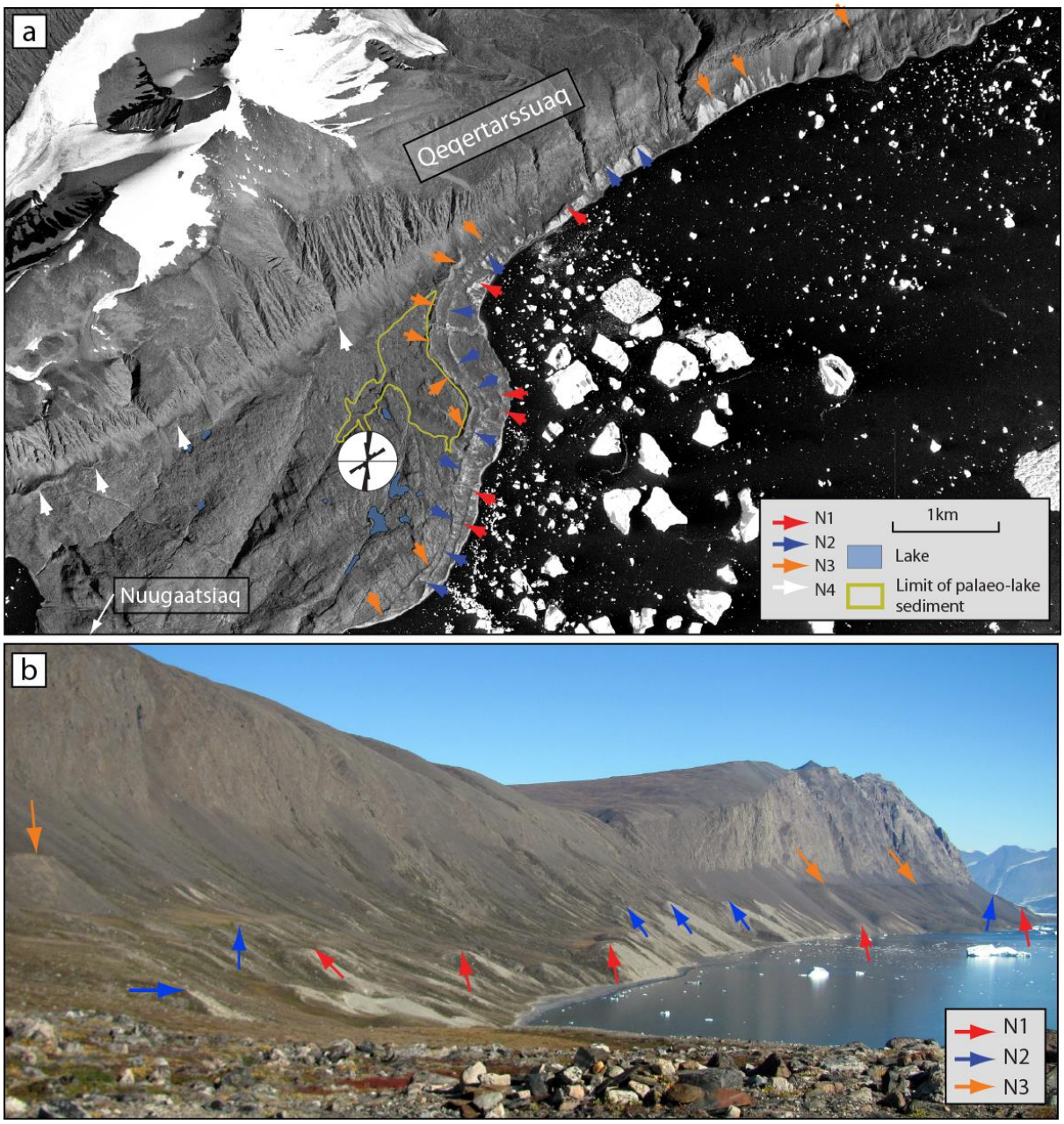

Figure 8. (a) Aerial photograph (from KMS) of the Nuugaatsiaq peninsula and fjord wall to the northeast. Striae data from 1040 m a.s.l are shown at the top right, and the high-altitude lateral push moraine is shown by black arrows. Fragments from each of the four inset lateral moraines (N1-4) are arrowed, and striae shown in a rose diagram (n=50). The hypothesised extent of lake sediment on the peninsula (based upon sediment distribution) is also outlined; (b) Photograph looking northeast of the continuation of the Nuugaatsiaq lateral moraine sequence (arrowed). The moraines are patchy, but can be traced for >5km.

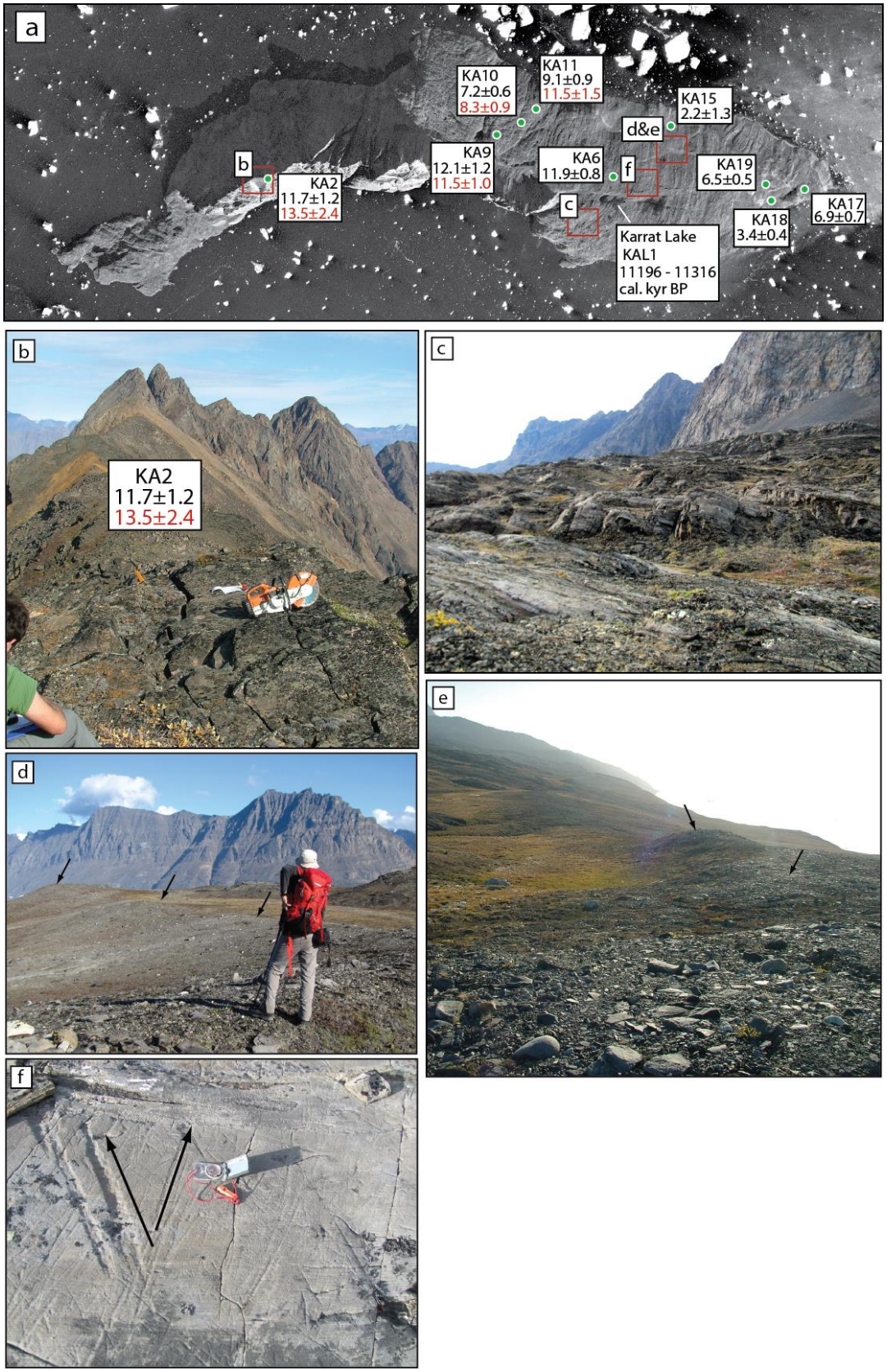

Figure 9. Plate of photographs from Karrat Island: (a) Aerial photograph of Karrat Island, showing the locations of Figures 10b-f. (b) *In situ* bedrock slab at 750 m a.s.l.; (c) Glacially polished roches moutonnées which are found ubiquitously across the east of the island at 200 m a.s.l.; (d and e) Views of K3, the outermost of the three moraines mapped on Karrat (210 m a.s.l); (f) Bi-directional striae from eastern Karrat (~255 m a.s.l.).

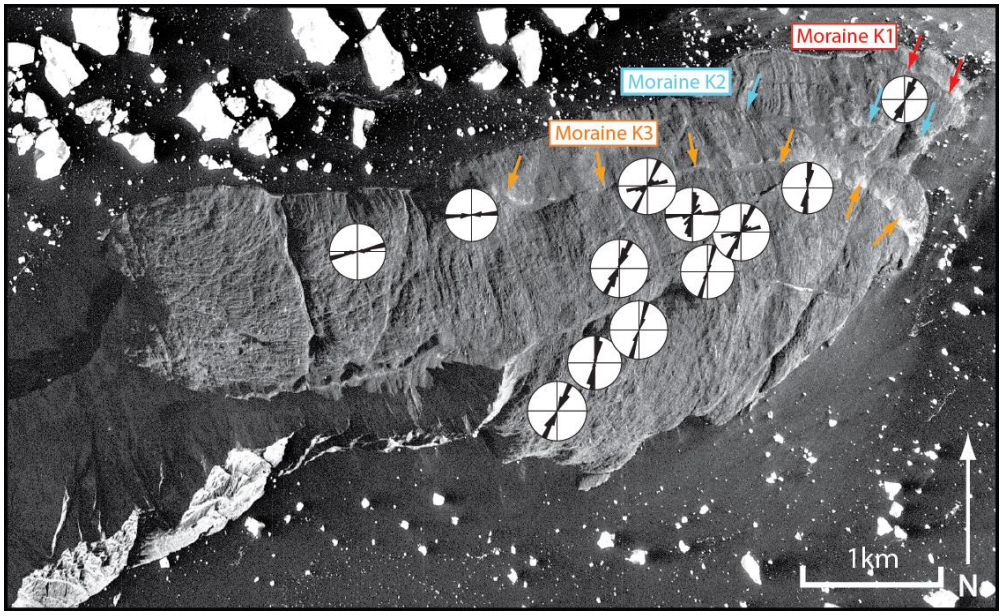

Figure 10. Aerial photograph of eastern Karrat, with Karrat moraines arrowed (K1-3). Superimposed rose diagrams show striae directions for a variety of locations across the island (n=50 for each location).

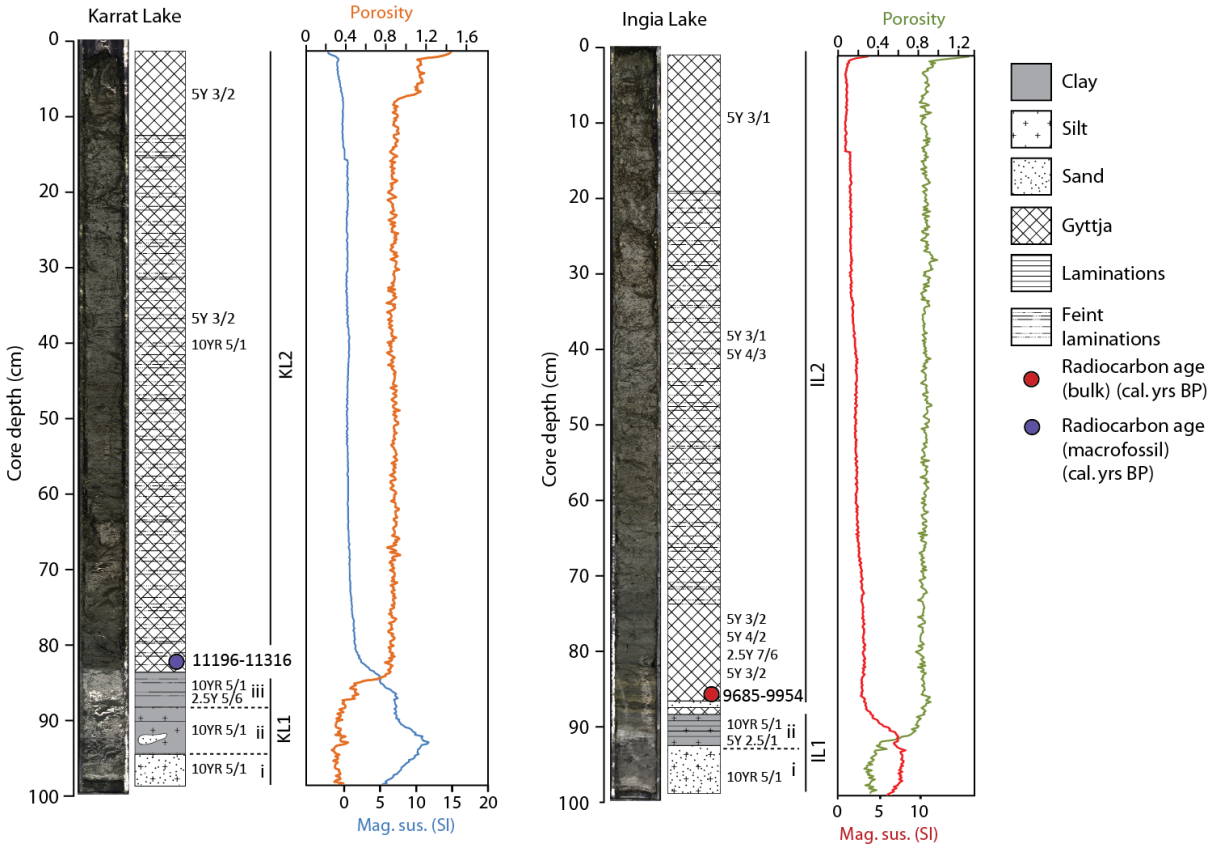

Figure 11. Photograph and sediment log of lake sediment cores from Karrat and Ingia Lake. Sedimentology is show diagrammatically, as is the location of basal ^{14}C dates taken. Note that the date from Karrat Lake is a bulk sample from lake gyttja, and the date from Ingia Lake is from a plant macrofossil. Magnetic susceptibility and porosity measurements are shown to the right of each core (measured using a Geotek Multi Sensor Core Logger).

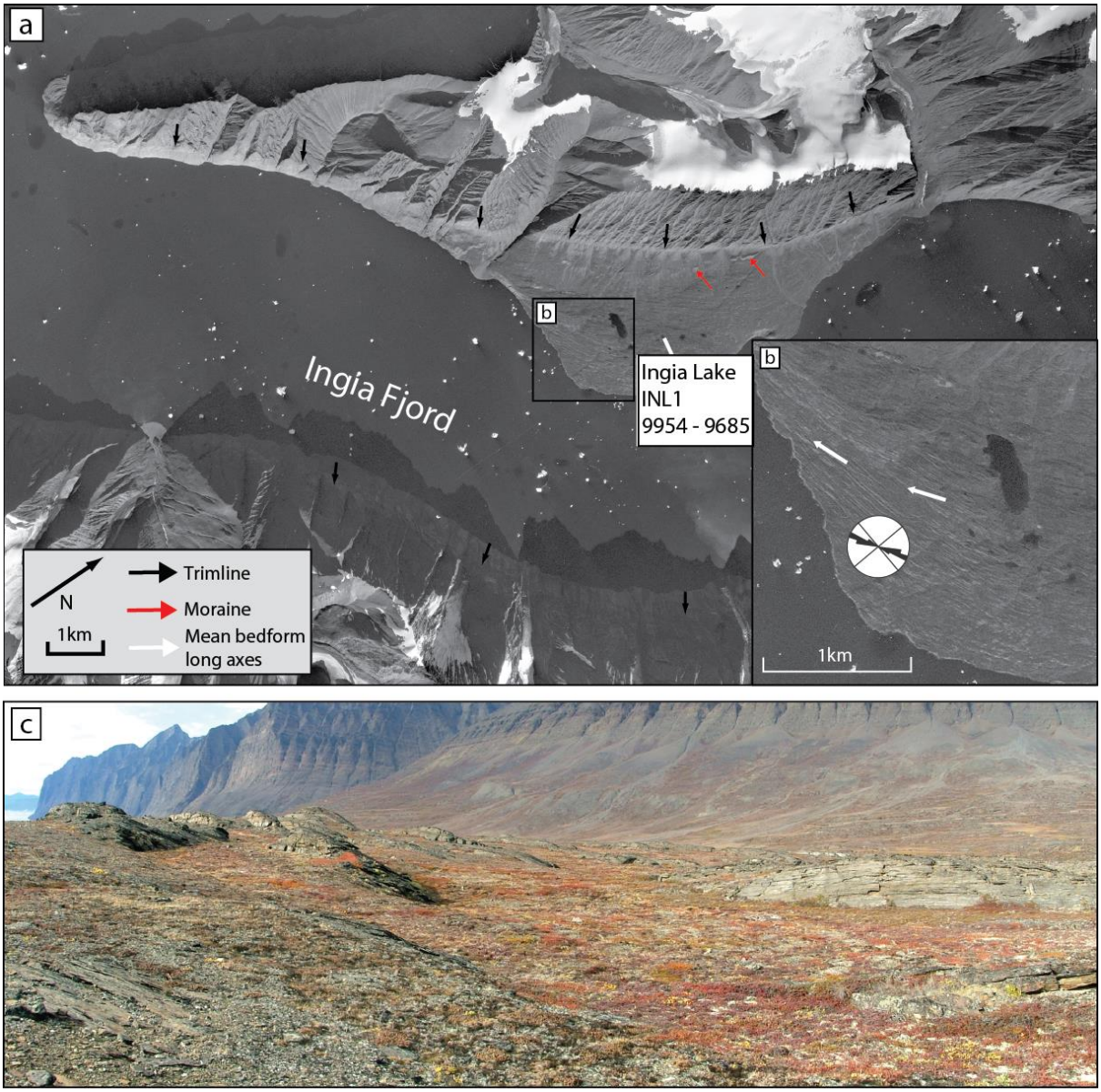

Figure 12. (a) Aerial photograph of Ingia Fjord (see Figure 4.3 for location). Black arrows mark the trimlines separated abraded surfaces from weathered, debris-rich surfaces above, red arrows indicate the fragmentary, partially rock glacierised lateral moraine. (b) Enlargement of the southwest portion of the peninsula, showing the ubiquitous glacially eroded whaleback and roches moutonnées. Average bedform long axes are shown by the white arrow, and striae are shown in a rose diagram (n=30). (c) Photograph of the landscape on the peninsula in Ingia Fjord. Photograph is taken looking west; south of the large lake visible in Figure 13b. Areally scoured terrain with large bedforms is visible in the fore- and mid-ground (ice-flow from right to left). Steep rock faces with gullies and associated talus cones are visible in the background. For scale, the bedform face to the right of picture is ~2 m high.

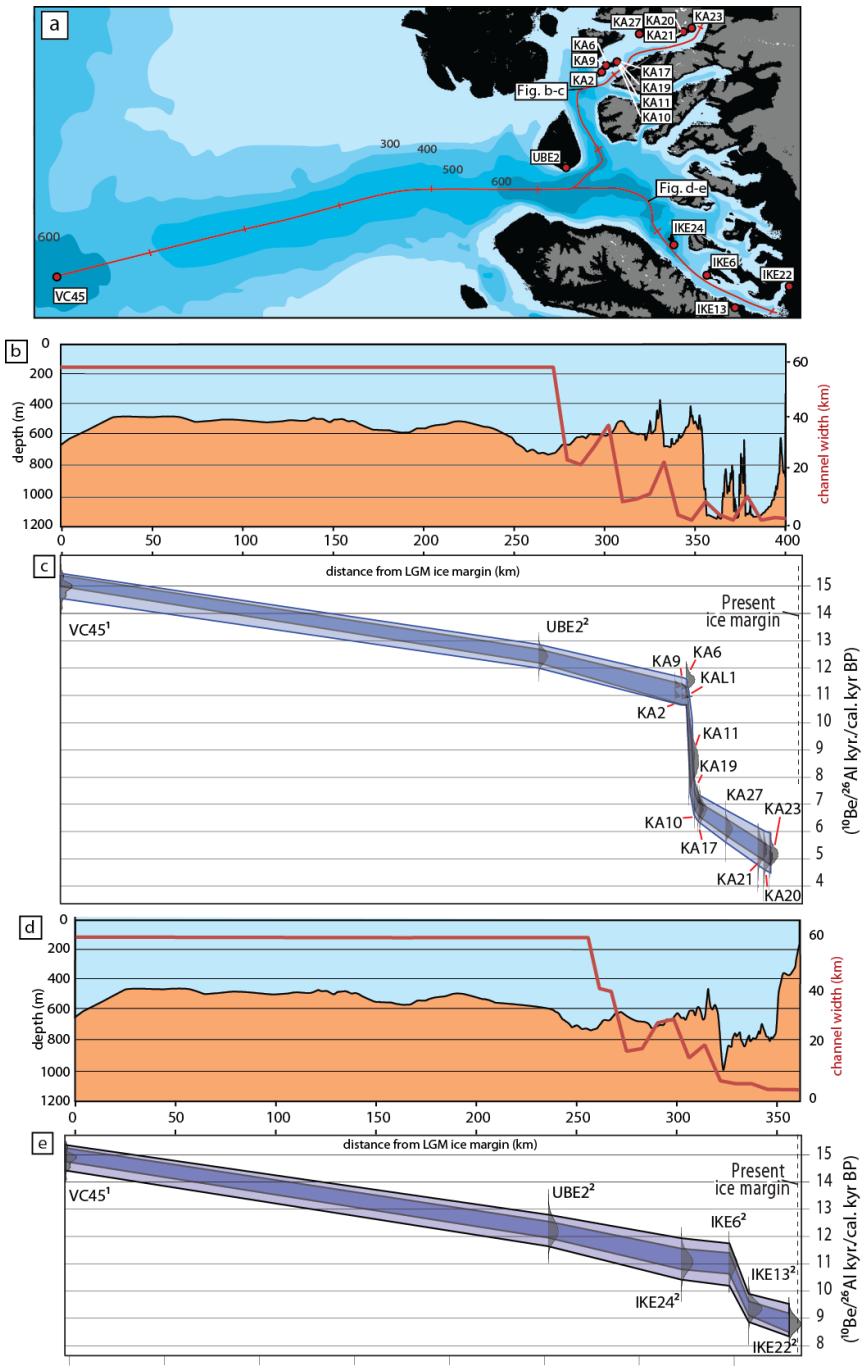

Figure 13. Sample locations, bathymetric profile, channel width, and dates from the northern UISS: (a) location of transects used in b and d, through the north and south of the Uummannaq region. Tick marks along each transect represent 50 km. Sample numbers are indicate to show location of samples in Figure 13c and e; (b) bathymetric profile through Uummannaq Trough, Igdlorssuit Sund, and Rink-Karrat Fjord using GEBCO and swath-bathymetry data (black line), and average channel width from the outer fjord to present margin (red line – measured manually); (c) Bayesian constrained age model of deglaciation through the northern Uummannaq region. Ages are from: [1]Ó Cofaigh et al., 2013b, [2]Roberts et al., 2013, and this study; (d) bathymetric profile through Uummannaq Trough, Igdlorssuit Sund, and the southern Uummannaq region using GEBCO and swath-bathymetry data (black line), and average channel width from the outer fjord to present margin (red line – measured manually); (e) Bayesian constrained age model of deglaciation through the southern Uummannaq region. Ages are from: [1]Ó Cofaigh et al., 2013b, [2]Roberts et al., 2013, and this study.

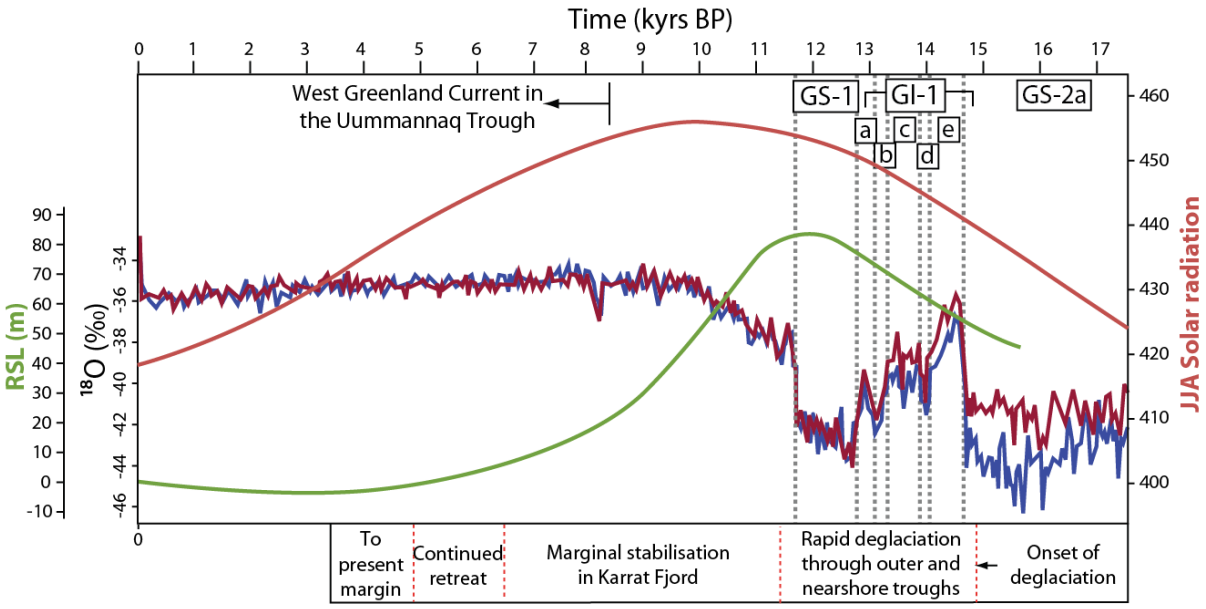

Figure 14. NGRIP (blue) and GRIP (red) δ18O record for the past 17 kyr (Lowe et al., 2008), relative sea-level curve from Arveprinsens Ejland (Long et al., 1999, Simpson et al., 2009), and JJA radiation for 70°N. Annotations below the figure show key events throughout the deglaciation of the north and south UISS. Labels refer to Greenland Stadial 1 (GS-1), Greenland Interstadial 1 (GI-1), and Greenland Stadial 2a (GS-2a) (Lowe et al., 2008).